# A 29-year time series of annual 300-metre resolution plant functional type maps for climate models

Kandice L. Harper[1], Céline Lamarche[1], Andrew Hartley[2], Philippe Peylin[3], Catherine Ottlé[3], Vladislav Bastrikov[3], Rodrigo San Martín[3], Sylvia I. Bohnenstengel[4], Grit Kirches[5], Martin Boettcher[5], Roman Shevchuk[5], Carsten Brockmann[5], Pierre Defourny[1]

[1]Earth and Life Institute, Université catholique de Louvain, 1348 Louvain-la-Neuve, Belgium
[2]Met Office Hadley Centre, Exeter, EX1 3PB, United Kingdom
[3]Laboratoire des Sciences du Climat et de l'Environnement, Institut Pierre-Simon Laplace, CEA-CNRS-Université Paris-Saclay, Orme des Merisiers, 91191 Gif-sur-Yvette, France
[4]Met Office, Reading, RG6 6BB, United Kingdom
[5]Brockmann Consult GmbH, 21029 Hamburg, Germany

*Correspondence to*: Céline Lamarche (celine.lamarche@uclouvain.be)

**Abstract.** The existing medium-resolution land cover time series produced under the European Space Agency's Climate Change Initiative provides 29 years (1992–2020) of annual land cover maps at 300-m resolution, allowing for a detailed study of land change dynamics over the contemporary era. Because models need two-dimensional parameters rather than two-dimensional land cover information, the land cover classes must be converted into model-appropriate plant functional types (PFTs) to apply this time series to Earth system and land surface models. The first generation cross-walking table that was presented with the land cover product prescribed pixel-level PFT fractional compositions that varied by land cover class but lacked spatial variability. Here we describe a new ready-to-use data product for climate modelling: spatially explicit annual maps of PFT fractional composition at 300 m resolution for 1992–2020, created by fusing the 300 m medium-resolution land cover product with several existing high-resolution datasets using a globally consistent method. In the resulting data product, which has 14 layers for each of the 29 years, pixel values at 300-m resolution indicate the percentage cover (0–100 %) for each of 14 PFTs, with pixel-level PFT composition exhibiting significant intra-class spatial variability at the global scale. We additionally present an updated version of the user tool that allows users to modify the baseline product (e.g., re-mapping, re-projection, PFT conversion, and spatial sub-setting) to meet individual needs. Finally, these new PFT maps have been used in two land surface models - ORCHIDEE and JULES - to demonstrate their benefit over the conventional maps based on a generic cross-walking table. Regional changes in the fractions of trees, short vegetation, and bare soil cover induce changes in surface properties, such as the albedo, leading to significant changes in surface turbulent fluxes, temperature, and vegetation carbon stocks.

## 1. Introduction

Terrestrial ecosystems have always been shaped by people who depend on land for their consumption of direct (e.g., food and materials) and indirect (e.g., land for human activities) goods (Vitousek et al., 1986; Foley et al., 2005). Land cover change induces significant biogeochemical and biogeophysical effects on the climate by altering greenhouse gas emissions (e.g., $CO_2$) and the surface energy budget, induced by modified albedo, evapotranspiration, and roughness (Pielke et al., 2011; Mahmood et al., 2014; Pielke, 2005; Brovkin et al., 2006; Dale, 1997; Liu et al., 2017). The fragmented landscapes that result from land cover change also influence surface temperatures, altering clouds and precipitation (Dale, 1997; Perugini et al., 2017; Sampaio et al., 2007). The physical climate changes driven by land cover change can manifest far afield of the surface changes; for example, large areas deforested at the expense of brighter land cover (e.g., cropland expansion) modify albedo (Loarie et al.,

40    2011; Lambin et al., 2001), with the altered energy balance driving changes in monsoon patterns (Feddema et al., 2005;
41    Devaraju et al., 2015).

42

43    Anthropogenic activities, driven mainly by economic and population growth (Pachauri and Meyer, 2014), have changed the
44    atmosphere's composition (IPCC, 2022). The land use, land-use change, and forestry sector is estimated to account for net
45    emissions of 4.1 $\pm$ 2.6 Gt $CO_2$ $yr^{-1}$ (1 $\sigma$ uncertainty, period 2011–2020), accounting for 10 % of total anthropogenic $CO_2$
46    emissions (Friedlingstein et al., 2022). The estimated net $CO_2$ emission uncertainty ($\pm$ 2.6 Gt $CO_2$ $yr^{-1}$) represents more than
47    50 % of the 10-year mean emission estimate and is the most uncertain emission component of the global carbon budget
48    (Friedlingstein et al., 2022; Houghton et al., 2012). Various sources contribute to this uncertainty, including differences in the
49    processes implemented in models (Bastos et al., 2020; Houghton et al., 2012; Pitman et al., 2009; McGlynn et al., 2022),
50    including the definition of the fluxes themselves (Pongratz et al., 2014) and the inclusion of management practices (Houghton
51    et al., 2012); the estimates of vegetation biomass density (Houghton, 2005); and estimates of land cover and rates of change
52    (Houghton et al., 2012; Bastos et al., 2021, 2020).

53

54    In support of the United Nations Framework Convention on Climate Change (UNFCCC) needs for observations of the climate
55    system, the Global Climate Observing System (GCOS) has identified 54 Essential Climate Variables (ECVs) that critically
56    contribute to improved characterization of the state of the global climate, making predictions of climate changes, and
57    performing attribution of the causes of such changes (GCOS, 2016). As a direct response, the European Space Agency (ESA)
58    launched the Climate Change Initiative (CCI) to provide stable, long-term, and consistent satellite climate data records
59    (Hollmann et al., 2013). The CCI thereby provides useful information to monitor the Paris Agreement goal of maintaining the
60    global temperature increase above pre-industrial levels to less than 2°C (UNFCCC, 2016).

61

62    Land cover, the observed biophysical cover of the Earth's surface (Di Gregorio and Jansen, 2005; Turner et al., 1993), is an
63    ECV (Sessa, 2008) tackled by the ESA CCI (Plummer et al., 2017). The ESA CCI medium-resolution land cover (MRLC)
64    dataset, operationalized within the EU Copernicus Climate Change Service (C3S) (2016-2020) thanks to strong user
65    endorsement, provides the longest consistent land cover climate data record, with annual maps from 1992 to 2020 at a spatial
66    resolution of 300 m. It describes the land surface in 22 land cover classes according to the standard of the United Nations Land
67    Cover Classification System (UN-LCCS) (Di Gregorio and Jansen, 2005) and 13 land cover change types consistent with the
68    IPCC land categories (Defourny et al., submitted).

69

70    The land surface components of global circulation models and global Earth system models play a significant role in quantifying
71    the historical and present-day representations of land use and land cover change impacts on climate. Most land surface models
72    (LSMs) parameterize global vegetation processes (e.g., photosynthesis and evapotranspiration) for a reduced set of globally
73    representative and similarly behaving plant types, referred to as Plant Functional Types (PFTs). PFTs can be related to
74    physiognomy and phenology (Anon, 1991 in Box, 1996), climate (which defines the geographical ranges in which a plant type
75    can grow and reproduce under natural conditions; Box, 1981), and physiological activity (e.g., $C_3/C_4$ photosynthetic pathways).

76

77    Spectral information acquired by remote sensing techniques does not allow direct mapping of PFTs. However, land cover map
78    series derived from satellite Earth Observations (EO) are a valuable source of physiognomy (life form and leaf type) and
79    phenology information for inferring the spatial distribution of PFTs. EO-derived land cover maps must be translated ("cross-
80    walked") into model-specific PFTs, which is typically accomplished using the information provided by the land cover class
81    legend (Jung et al., 2006). Differences in land cover categories, spatial resolutions, and temporal coverage between various
82    land cover products propagate errors to the cross-walked PFT maps and significantly contribute to uncertainties in deriving

gross primary production (GPP) and other climate-relevant variables at the regional scale (Poulter et al., 2011). To reduce uncertainty in model ensembles, Poulter et al. (2015) proposed a standardized cross-walking framework that converts each CCI MRLC class into pre-defined PFT fractions relevant for three leading ESMs (JULES-MOHC, ORCHIDEE-LSCE and JSBACH-MPI) based on expert knowledge and auxiliary data. This reclassification procedure was implemented in a flexible tool to generate other related PFT schemes required by the modelling community.

Hartley et al. (2017) used the same three ESMs to quantify the impact of uncertainties in (1) the land cover map and (2) the cross-walking procedure on the spatio-temporal patterns of three important land surface variables: GPP, evapotranspiration, and albedo. To disentangle the two sources of uncertainty, the modelling setup translated the plausible uncertainty ranges of the land cover and cross-walking components into a common biomass scale. The simulations indicated that the uncertainty of the cross-walking procedure contributed slightly more than the uncertainty of the land cover map to the inter-model uncertainty for all three variables.

In a continuation of the ESA CCI contribution to the land cover ECV, this work aims to reduce the uncertainty in the cross-walking component    by adding spatial variability to the PFT composition within a land cover class. This work moves beyond fine-tuning the cross-walking approach for specific land cover classes and/or regions and, instead, separately quantifies the PFT fractional composition for each 300 m pixel globally for each year in the time series (1992–2020). The new PFT product is generated by fusing the annual CCI MRLC map series with existing high-resolution auxiliary data products that individually characterize one surface type with high accuracy. The resulting 300 m PFT product is a companion time series of continuous field PFT fractions that is consistent with the existing CCI MRLC map series. The global PFT product has an annual resolution, covering 1992–2020, and indicates the specific percentage cover of 14 PFTs for each pixel at 300 m resolution. The set of 14 PFTs represented in the product includes the full set of 13 PFTs initially developed by Poulter et al. (2015) complemented with a new built-up surface type. The full set of PFTs includes bare soil, built, water, snow and ice, natural grasses, managed grasses (i.e., herbaceous cropland), broadleaved deciduous trees, broadleaved evergreen trees, needleleaved deciduous trees, needleleaved evergreen trees, broadleaved deciduous shrubs, broadleaved evergreen shrubs, needleleaved deciduous shrubs, and needleleaved evergreen shrubs. Thus, in this paper, the term "plant functional type" is applied even to the abiotic surface types to cleanly differentiate between the land types derived from Earth observation data (i.e., land cover classes) and the land types required by models (i.e., PFTs). Finally, these new PFT maps have been used in two land surface models (ORCHIDEE and JULES) to demonstrate their benefit over the conventional maps based on a generic cross-walking table. For brevity, the new PFT product is referred to as "PFT$_{local}$" due to the new localised nature of the PFT fractions at the pixel level. Products derived by using the global cross-walking approach (using the same version 2.0.8 of the CCI MRLC map series) are referred to as "PFT$_{global}$."

The following sections describe the auxiliary inputs and method used to quantitatively determine the PFT fractional composition for each 300 m pixel globally; a description of the new PFT data product; and modelling results from the application of the new PFT distribution for the year 2010 to the ORCHIDEE and JULES land surface models.

## 2.    Methods

The PFT distribution was created by combining auxiliary data products with the CCI MRLC map series. The land cover classification provides the broad characteristics of the 300 m pixel, including the expected vegetation form(s) (tree, shrub, grass) and/or abiotic land type(s) (water, bare area, snow and ice, built-up) in the pixel. For some classes, the class legend specifies an expected range for the fractional covers of the contributing PFTs and broadly differentiates between natural and

124  cultivated vegetation. The applied auxiliary data products (described in Sect. 2.1; e.g., surface water cover and tree cover) are
125  of higher resolution than the 300 m land cover product and therefore serve as the basis for computing the fractional covers of
126  the contributing PFTs at 300 m resolution. In cases of inconsistency between the land cover product and the auxiliary datasets
127  – for example, if the tree cover percentage derived from the auxiliary products falls outside of the range suggested by the class
128  legend for a 300 m pixel – the characteristics from the land cover classification are maintained. This achieves a strong coupling
129  between the CCI MRLC maps dataset and this new CCI PFT dataset. Deference to the class legend provides guardrails for the
130  temporal extrapolation of the PFT fractional covers across the entire time series (1992–2020) given the lack of available
131  auxiliary inputs extending across the full era. The approaches used to estimate the PFT fractions at 300 m resolution differ for
132  (1) pixels that did not experience a change in land cover classification over the period 1992–2020 (termed "static pixels",
133  described in Sect. 2.2.1) and (2) pixels that did experience a change at least once in this period (termed "change pixels",
134  described in Sect. 2.2.2).

## 2.1. Input datasets

### 2.1.1. CCI medium-resolution land cover time series (300 m)

137  The CCI MRLC product (Defourny et al., submitted) delineates 22 primary classes and 15 additional sub-classes of land cover
138  at a 10-arcsecond (300 m) resolution (**Table 1**). The maps have global coverage and an annual time step extending from 1992
139  through 2020, with plans for the continued release of maps for 2021 and future years. The classification system used for the
140  CCI MRLC map series is based on the Land Cover Classification System (LCCS) of the United Nations Food and Agriculture
141  Organization (UN FAO) (Di Gregorio and Jansen, 2005). The LCCS defines fundamental landscape elements called
142  "classifiers" (e.g., trees) forming the class legend when combined in various proportions (e.g. tree cover, broadleaved,
143  evergreen, closed to open (>15 %)). The 15 sub-classes, also called "regional classes," are defined only in geographic regions
144  where appropriate training data is available and are those with a numeric classification code that has a final digit of 1, 2, or 3
145  (**Table 1**). The 22 primary classes and 15 sub-classes are collectively referred to here as simply "classes." For each year of the
146  time series, each 300 m pixel in the dataset is assigned as a single land cover class. The change detection algorithm monitors
147  thirteen possible land cover transitions through time. For a pixel to register a change in its assigned land cover class, the
148  algorithm must identify the change for two consecutive years in the workflow. A lack of change in a pixel's assigned class
149  does not necessarily indicate an absence of change in the land surface over the time series; rather, it indicates that any change
150  that has occurred in the pixel was limited enough in scale or duration that the assigned class did not change. The full time
151  series and an associated set of quality flags are freely available at https://maps.elie.ucl.ac.be/CCI/viewer/ (last access August
152  2022) in GeoTiff and https://cds.climate.copernicus.eu/cdsapp#!/dataset/satellite-land-cover?tab=overview (last access
153  August 2022) in netCDF. This CCI PFT product is based on v2.0.8 of the CCI MRLC time series, which includes corrections
154  for the known overestimation of cropland relative to grassland in South America (Defourny et al., submitted).

### 2.1.2. Surface water product (30 m)

156  The Landsat-based surface water product developed by the Joint Research Centre (Pekel et al., 2016) is used to derive the
157  permanent inland water fractions at 300 m resolution (calculation details in Sect. 2.2). The surface water occurrence layer
158  (obtained at https://global-surface-water.appspot.com) indicates the frequency of water occurrence in each 30 m pixel (80°N–
159  60°S) over the period March 1984 to December 2019. The frequency occurrence data is reported as integer values of 1–100
160  %, where a value of 100 % occurrence indicates a permanent water surface that existed over the entire analysis period, which
161  encompasses all but the most recent year (2020) of the time series of the MRLC product.

### 2.1.3. Tree canopy cover product (30 m)

A Landsat-based tree canopy cover product (Hansen et al., 2013) is used to derive the tree cover fractions for 300 m pixels belonging to vegetated classes (except where otherwise noted in Sect. 2.2). The product (obtained at https://glad.umd.edu/Potapov/TCC_2010/) is based on the application of a regression tree model to growing-season Landsat 7 ETM+ data (https://glad.umd.edu/dataset/global-2010-tree-cover-30-m). The dataset indicates the maximum tree canopy cover percentage (integer values of 1–100 %) at 30 m resolution (80°N–60°S) and is approximately representative of 2010.

### 2.1.4. Tree canopy height product (30 m)

The global forest canopy height product from Potapov et al. (2021) is used to derive the fractional covers of trees and shrubs in 300 m pixels classified as shrubland. The 30 m product (obtained at https://glad.umd.edu/dataset/gedi/) was created by combining the footprint-level lidar forest height measurements (using the 95th percentile relative height metric) for April–October 2019 from the Global Ecosystem Dynamics Investigation with wall-to-wall Landsat optical data to perform spatiotemporal extrapolation. The resulting dataset indicates the canopy height (0–60 m) at 30 m resolution (52°N–52°S), where canopy heights < 3 m were set to 0 m under the assumption that the pixel lacks woody vegetation.

### 2.1.5. Built-up product (38 m)

The Landsat-based Global Human Settlement Layer (GHSL) dataset produced by the Joint Research Centre (Pesaresi et al., 2013) is used to derive the built-up fraction for 300 m pixels classified as urban land cover by the Global Urban Footprint (GUF) dataset (Esch et al., 2017). The built-up fraction of the PFT dataset is defined as buildings, roads, and man-made structures. The GHSL (alpha version dated November 2014) consists of globally consistent built-up maps for four consecutive years (1975, 1992, 2000, and 2014) at 38 m resolution. Built-up areas include both permanent and temporary above-ground buildings.

### 2.1.6. Zonation products

In addition, three zonation products are used complementarily to consolidate the assignment of the phenology type (deciduous or evergreen) and leaf type (broadleaved or needleleaved) to shrubs and, in a very small number of pixels, to trees belonging to a class legend of mixed trees. The Köppen-Geiger climate zone product from Beck et al. (2018) divides the Earth's land surface into 30 distinct climate zones at 0.0083° resolution (about 1 km) based on present-day (1980–2016) temperature and precipitation records. Data were obtained at https://figshare.com/articles/dataset/Present_and_future_K_ppen-Geiger_climate_classification_maps_at_1-km_resolution/6396959/2. The landform dataset from Sayre et al. (2014) identifies landforms – surface water, plains, hills, or mountains – at 250 m resolution for 83.6°N–56°S and is derived from a digital elevation model (USGS GMTED2010: Danielson and Gesch, 2011). The data product was obtained at https://rmgsc.cr.usgs.gov/outgoing/ecosystems/Global/. Finally, world regions follow the definitions used in the Integrated Model to Assess the Global Environment 3.0 (IMAGE03) (Stehfest et al., 2014). The IMAGE03 regional classification framework has been harmonized with the CCI MRLC grid by reconstructing the original dataset using the IMAGE-based list of countries per region (available at https://models.pbl.nl/image/index.php/Region_classification_map) along with country boundaries from the FAO Global Administrative Unit Layers (available at https://data.apps.fao.org/), expanding the list to include Antarctica, Greenland, and additional small islands. The resulting raster dataset divides Earth's surface into 28 regions on the CCI MRLC grid.

### 2.1.7. CCI medium-resolution water body product

The CCI MRLC water body product (Lamarche et al., 2017) is used to delineate between inland water and ocean. The dataset (available at http://maps.elie.ucl.ac.be/CCI/viewer/download.php) designates all pixels at 150 m resolution as either ocean or non-ocean, the latter of which includes both land and inland water. The dataset is consistent with the water body class (code 210) of the land cover maps of the CCI MRLC. An updated version 4.1 of the product was used here, in which the North American Great Lakes are now considered to be inland water rather than ocean. It is available at http://maps.elie.ucl.ac.be/CCI/viewer/download.php.

## 2.2. PFT dataset development

The overall approach assumes that the definition of the MRLC class is the basis for harmonizing the four existing high-resolution land cover data sets. It proceeds through a systematic sequence of estimating water fraction and tree cover fraction, using tree height to assign life form, and finally deriving phenology. This step-by-step approach is first applied to static pixels before extending it to pixels that undergo changes over time, as identified in the CCI MRLC map series.

### 2.2.1. Static pixels

For static pixels – that is, pixels that have not experienced a class change over the era covered by the CCI MRLC time series (1992–2020) – the derived PFT fractions are treated as temporally invariant for the entire period. Therefore, any intra-pixel change in the fractions of a static pixel is not captured in the PFT map series due to a lack of temporally resolved auxiliary inputs extending over the full time series. Such a change is expected to be so limited in scale and/or duration that it did not prompt a change in class assignment, underscoring the appropriateness of treating the fractional composition of the static pixels as consistent over time.

The same set of auxiliary inputs and the same calculation method are applied to the widest possible set of land cover classes to ensure spatial consistency in the derived PFT fractions. Nonetheless, inherent differences between the classes necessitate the use of different input datasets and methods in some cases. For each class, only a subset of the 14 PFTs is permitted non-zero fractions (**Table 1**). Because the PFT fractional composition is estimated independently for each 300 m pixel of a class, in some cases, an individual pixel of the class can have zero fractional cover even for a PFT that is allowed non-zero cover for that class. For all pixels, the sum of PFT fractions is 100 %. The vegetation thresholds used to define whether pixels are predominantly vegetated or abiotic are based on the definitions of the CCI MRLC classes, which are based on the concepts and definitions of the FAO LCCS (Di Gregorio and Jansen, 2005). Table 2 is a high-level overview of the method used to derive the PFT fractional composition for the static pixels.

The 30 m water frequency occurrence dataset of Pekel et al. (2016) is used to estimate the permanent inland water fraction of the 300 m pixels for all but the permanent snow and ice class, which has no liquid surface water cover. A threshold of 90 % frequency occurrence is applied to assign 30 m pixels as either water (frequency occurrence $\geq$ 90 %) or non-water (frequency occurrence < 90 %). The resulting binary representation of water/non-water is aggregated to 300 m to estimate the percentage of the 300 m pixel that is permanent inland water PFT.

The percentage of the 300 m pixel that is vegetated is calculated as 100 % minus the inland water percentage; that is, for all vegetation-containing classes except for the sparse vegetation classes, which have bare soil PFT cover, all non-inland-water area in the 300 m pixel is entirely vegetated (0 % bare soil PFT) in the PFT product. Pixels belonging to the shrubland classes

(codes 120–122 and 180) can have a mixture of trees, shrubs, and herbaceous cover. For pixels of non-shrubland vegetation-containing classes, the vegetated portion of the pixel is composed of trees and herbaceous cover (i.e., cropland and/or natural grass). The percentage of the 300 m pixel that is tree cover is estimated using the 30 m tree cover dataset for 2010 from Hansen et al. (2013). This Landsat-based dataset provides the percentage of tree canopy cover (integers 1–100 %) based on growing season observations. The tree cover percentage of the vegetated (i.e., non-water) portion of the 300 m pixel is obtained from the median of the tree canopy cover fractions of the non-water 30 m pixels, where the 30 m non-water pixels are identified using the binary water/non-water representation derived using the surface water occurrence dataset. The tree cover percentage of the entire 300 m pixel is calculated as the product of this value (the tree cover fraction of the non-water part of the grid cell) and the non-water fraction of the grid cell. This approach harmonizes the Landsat-based surface water occurrence and tree canopy cover datasets such that the combined tree and water percentages never exceed 100 %.

For the tree cover classes 50–82, the class legend specifies an expected range for the tree cover percentage (**Table 1**, class description column). For the tree cover classes 90, 160, and 170, a tree cover fraction of >15 % is implicit from the UN LCCS. Based on the spatial and temporal consistency of the map series, deference is made to the class legend for pixels in which the estimated tree cover fraction derived from the auxiliary datasets disagrees with the class legend. This allows the PFT product to retain the advantages of the CCI MRLC map series while improving the translation of the land cover dataset into PFT maps. For tree cover class pixels in which the estimated tree cover fraction derived from the auxiliary datasets disagrees with the class legend, the mean tree cover among all static 300 m pixels of its class is calculated over the 0.25° longitude × 0.25° latitude window overlapping the pixel – that is, a window with width and height of 0.25° with the pixel of interest at the centre. The mean is based on the initially calculated tree cover fractions derived from the auxiliary data products (i.e., the tree cover fraction harmonized with the surface water occurrence dataset). The window is expanded to 0.5° longitude × 0.5° latitude if no static pixels of the class exist in the smaller window. (Because class 82 has so few pixels globally, class 72 pixels are additionally applied in the window mean calculation for class 82 pixels.)

One of five cases is possible:

(1) If the mean tree fraction for the window falls within the expected range based on the class legend, then the tree cover fraction of the pixel of interest is assigned as the mean tree fraction for the window.
(2) If the mean tree fraction for the window is higher than the upper limit specified by the class legend, then the tree cover fraction of the pixel of interest is assigned as the upper limit from the legend. For classes 62, 72, and 82, the legend upper limit is 40%. For classes 50, 60, 61, 70, 71, 80, 81, 90, 160, and 170, the legend upper limit is 100 %, and the initial mean tree fraction for the window can never exceed this threshold.
(3) If the mean tree fraction for the window is lower than the lower limit specified by the class legend, then the tree cover fraction of the pixel of interest is assigned as the lower limit from the legend. For classes 50, 60, 62, 70, 72, 80, 82, 90, 160, and 170, the legend lower limit is 16 %. For classes 61, 71, and 81, the legend lower limit is 41 %.
(4) If a window of 0.5° × 0.5° does not have any pixels of the class of interest and the tree cover fraction derived from the auxiliary products exceeds the upper limit specified by the class legend, then the tree cover fraction for the pixel is assigned as the upper limit of the class legend.
(5) If a window of 0.5° × 0.5° does not have any pixels of the class of interest and the tree cover fraction derived from the auxiliary products is lower than the lower limit specified by the class legend, then the tree cover fraction for the pixel is assigned as the lower limit of the class legend.

For pixels that belong to a tree cover class and had tree cover percentages assigned using the neighbourhood mean, the resulting sum of the inland water and tree cover percentages can exceed 100 %. In such cases, the tree cover percentage is calculated as 100 % minus the inland water percentage. If the resulting tree cover percentage is lower than the legend minimum for that class, then the tree cover percentage is set as the legend minimum and the water percentage is set as the residual area in the pixel (100 % minus tree cover percentage). For all tree cover class pixels, the grass cover percentage is calculated as 100 % minus the final tree cover percentage minus the inland water percentage, and the grass type is assigned as natural grasses. No minimum water percentage is defined for the flooded tree cover classes (codes 160 and 170).

For the biotic classes rainfed cropland (codes 10, 11, 12), irrigated or post-flooding cropland (code 20), mosaic of cropland–natural vegetation (codes 30 and 40), mosaic of woody–herbaceous vegetation (codes 100 and 110), and grassland (code 130), the tree cover percentage derived from the auxiliary products is used directly since the legend does not specifically define the expected tree cover; therefore, modification of the PFT fractions based on the class legend is not applied for these classes as it is for some other classes. The percentage of the 300 m pixel that is grass cover is calculated as 100 % minus the sum of the inland water and tree cover percentages. The grass type – managed (i.e., crops) or natural – is defined by the class legend. For most mixed classes, the assigned grass type reflects the majority type as indicated by the legend. All grass in the pixel is assigned as managed grass for classes 10, 11, 12, 20, and 30. Pixels belonging to the mosaic class 40 have a mix of herbaceous crops (up to 49 % of the pixel area) and natural grasses (for excess grass cover beyond 49 % of the pixel area). All grass cover is assigned as natural grass for all other classes.

In some of the classes in this set, an expected percentage cover is given for total woody vegetation (trees and shrubs) or for the shares of cropland and natural vegetation, where the two categories differentiate by management status rather than life form. In the PFT product, shrub cover is estimated only for the shrubland classes due to a lack of appropriate auxiliary inputs to discriminate between trees and shrubs for all classes, so modification of the life form shares in such pixels based on the legend description may introduce additional bias in the PFT product and is therefore avoided. Management status (cropland vs natural) is assigned in the PFT product only for grasses and is based on the class descriptions, so an independent assessment of the shares by management status is not possible.

Pixels belonging to the sparse vegetation classes (codes 150, 151, 152, and 153) can have non-zero fractions of bare soil, trees, natural grass, and inland water. The class definition requires a vegetation fraction of 4–14 %. Since shrub cover is not estimated for the sparse vegetation classes, the vegetation component is composed of trees and natural grasses; therefore, the total vegetation fraction is enforced for sparse vegetation pixels, but the resulting life form may differ from that indicated by the legend for the sub-classes with codes 151–153. If the tree cover derived from the auxiliary inputs is ≥ 15 %, then the tree PFT is reduced to 14 % in deference to the legend of the CCI MRLC map series, natural grass PFT is assigned as 0 % since tree cover accounts for the maximum total vegetation fraction (trees + grass), and the bare soil PFT percentage is calculated as 100 % minus the inland water percentage minus 14 % tree PFT. If the tree cover derived from the auxiliary inputs is < 15 %, then this input tree percentage value is assigned as the final tree PFT percentage in the pixel and additional legend-consistency steps are applied to assign the grass and bare fractions: (1) if the non-water area of the pixel is 4–14 %, then natural grass PFT accounts for the residual portion of the pixel (14 % minus tree PFT percentage minus inland water percentage); (2) if the non-water percentage of the pixel is < 4 %, then the natural grass PFT percentage is calculated as 4 % minus the tree PFT percentage (since the lower bound on total vegetation is 4 %) and the water PFT percentage is scaled down to 96 %; or (3) if the non-water percentage of the grid cell exceeds 14 %, then the natural grass percentage is calculated as 14 % minus the tree PFT percentage (that is, the upper bound of 14 % is assumed for total vegetation cover) and the residual pixel area is assigned as bare soil PFT (100 % minus water PFT percentage minus 14 % vegetation cover).

A mixture of tree and shrub woody vegetation types is assigned to pixels of the shrubland classes (codes 120, 121, 122, and 180). The 30 m resolution tree canopy height dataset from Potapov et al. (2021) is applied to discriminate between shrubs and trees in pixels that are covered by this data product (52°N–52°S). Potapov et al. (2021) re-assign pixel values of ≤ 2 m to 0 m height. Here, the 30 m resolution pixels are assigned to three broad height classes: 0 m, 3–5 m, and > 5 m. Mean re-sampling to the 300 m resolution of the land cover dataset results in pixel values that indicate the percentage cover of the three height classes. The percentage cover of the 3–5 m height class is taken to be the percentage shrub cover in the 300 m pixel and the

percentage cover of the > 5 m height class is taken to be the percentage tree cover in the 300 m pixel, recognizing that there may be some bias introduced by 30 m pixels in the input dataset that contain both shrubs and trees. In deference to the class legend, 300 m pixels with shrub cover < 16 % are assigned as having 16 % shrub cover and those with tree cover > 15 % are assigned as having 16 % tree cover. For shrubland pixels that occur outside of the extent of the Potapov et al. (2021) data product (52°N–52°S), the tree cover percentage is assigned according to the tree cover input derived from Hansen et al. (2013) and the shrub cover percentage is assigned following the most recent version of the global cross-walking table (CWT) (60 % shrub cover for classes 120–122 and 40 % shrub cover for class 180). For all shrubland pixels, in cases where the sum of water, tree, and shrub cover exceeds 100 %, the three PFTs are scaled down proportionally so that the sum is 100 % while retaining the legend expectations for the tree and shrub cover. Natural grass cover is assigned as the residual area of the pixel in cases where the sum of water, tree, and shrub cover is < 100 %. No minimum water percentage is defined for the flooded shrubland class (code 180).

Pixels classified as urban (code 190) can have non-zero fractions of inland water, trees, natural grass, and urban impervious (built-up) PFTs. In the land cover classification, pixels are assigned as an urban class when a minimum threshold of 50 % built was exceeded based on the GUF dataset (Esch et al., 2017). In the PFT product, the tree and surface water fractions are derived using the same protocol as the one applied to the vegetated classes. The urban impervious fraction is derived from the GHSL dataset (Pesaresi et al., 2013) by aggregating the built-up pixels from the four epochs into a binary built-up / non-built-up distribution at 38 m. Re-sampling to 300 m provides the percentage of the 300 m pixel that is built PFT, introducing local variability which at the global scale ranges from 0–100 % built. Only pixels classed as urban by GUF are assigned a non-zero urban impervious fraction in the PFT dataset. Non-urban pixels (i.e., those with less than 50 % urban land cover according to GUF) are not refined with GHSL data or assigned a percentage built-up. The GHSL appears to capture urban impervious areas more consistently whereas GUF misses road fractions in the built fractions. This is most notable in rural areas and a few selected locations in city centres. If the sum of the urban impervious, tree, and water fractions exceeds 100 %, then the urban impervious percentage is retained and the water and tree percentages are scaled down proportionally to a total sum of 100 %; otherwise, the residual of the urban impervious, tree, and water percentages is assigned as the natural grass percentage.

Water body class (code 210) pixels that are ocean are assigned as 100 % water PFT, while those that are inland can additionally have a non-zero cover of tree and natural grass PFTs. The designation of ocean vs. inland at 300 m is determined using the 150 m water body product. The ocean designation is applied to water body class pixels in which all four of the overlapping 150 m pixels of the water body product are classified as the ocean; all other water body class pixels are designated as inland water. The water and tree PFT fractions for inland water body class pixels are assigned using the same 300 m harmonized surface water and tree cover auxiliary inputs that are used for the other classes; however, a minimum of 86 % water PFT is enforced following the legend definition for this class. If the sum of the tree fraction and the adjusted water PFT fraction exceeds 100 %, then the tree percentage is scaled down as 100 % minus the adjusted water PFT percentage. Any residual area is assigned as natural grass PFT.

The bare area classes (codes 200, 201, and 202) can have up to 3 % vegetation cover (by definition of the abiotic class in the FAO LCCS; Di Gregorio and Jansen, 2005), so bare area pixels can have non-zero fractions of bare soil, tree, and water PFTs. The auxiliary products define the tree and inland water fractions, but tree cover exceeding 3 % is scaled down to the class maximum of 3 %. Bare soil PFT percentage is calculated as 100 % minus the inland water percentage minus the tree percentage. Pixels of the mosses and lichens class (code 140) can have non-zero fractions of surface water and natural grasses, the latter of which is estimated as 100 % minus the inland water percentage.

The permanent snow and ice class (code 220) is assigned as 100 % snow and ice PFT. All other classes are assigned as 0 % snow and ice PFT. Nearly all pixels classified as permanent snow and ice class in the CCI MRLC time series are static pixels; that is, such pixels are snow and ice cover for every year of the land cover map series. This is due to a lack of temporally resolved input data available at the global scale to track the evolution of this surface type. Therefore, neither the CCI MRLC classification nor the associated PFT product should be used to track changes in glaciers over time.

For all pixels – of any class – that have a non-zero tree fraction, the total tree fraction is assigned as a single tree type (broadleaved or needleleaved leaf type, deciduous or evergreen phenology). For the tree cover classes coded 50–82, the specific tree type follows the class legend. For example, class 50 is defined as "Tree cover – broadleaved evergreen >15 %," so the tree component of this class is assigned as the broadleaved evergreen tree type. Tree cover is assigned as broadleaved deciduous in pixels of classes 60–62, needleleaved evergreen in pixels of classes 70–72, and needleleaved deciduous in pixels of classes 80–82. For pixels of the tree cover classes coded 90, 160, and 170 and all other vegetation-containing classes except the shrubland classes, the specific tree type is assigned by pixel based on the majority tree type in the surrounding $0.25° \times 0.25°$ neighbourhood window, where the majority calculation is performed on static pixels of the tree cover classes with legend-defined tree types (classes 50–82). If the $0.25° \times 0.25°$ window does not contain any static pixels of the well-defined tree types, then the window is incrementally expanded by $0.25°$ in each direction (longitude and latitude) to a maximum window size of $2° \times 2°$ until such a pixel is contained within the search window. The same tree type is assigned to all pixels in a class for the tree cover classes 50–82, while the assigned tree type can vary between pixels within a class for the other classes. The vast majority (75 %) of pixels with a non-zero tree fraction were assigned a tree type directly using the class legend; an additional 24 % had tree type assigned using a surrounding window of $0.25° \times 0.25°$, < 1 % using a larger window up to a size of $1° \times 1°$, and < 0.1 % using an even larger window up to a size of $2° \times 2°$.

For a very small number of pixels, static pixels of the type-defined tree cover classes are absent from the surrounding $2° \times 2°$ window, so a climatological approach is instead used to assign the tree type to such pixels. This approach uses three auxiliary inputs: (1) the present-day Köppen-Geiger climate zone map from Beck et al. (2018), downscaled from 1 km resolution to the 300 m CCI MRLC grid using mode resampling; (2) the map of world regions derived for use with the IMAGE03 model, expanded to include Greenland, Antarctica, and additional small islands; and (3) the landform map from Sayre et al. (2014), resampled from 250 m resolution to the 300 m CCI MRLC grid using mode resampling. A nearest neighbour analysis is used to gap fill missing data at 300 m resolution for each of the three auxiliary inputs. Pixels requiring data are those with < 100 % water PFT cover in the PFT product. Pixels that are designated as surface water in the landform dataset and have < 100 % water PFT cover in the PFT product are additionally filled with one of the terrestrial landforms (plains, hills, and mountains). Missing data generally occur along coastlines due to mismatches in the land-sea masks of the auxiliary datasets and the CCI MRLC data. The gap-filled datasets are combined to create a dataset of 1,531 unique combinations of landform, region, and climate zone. For each of the unique combinations, the areal cover of each of the tree cover classes with well-defined tree types (codes 50–82) is calculated using static pixels of those classes, and the majority tree type by area is identified for each unique combination. There are very few static pixels of the type-defined tree cover classes in the Middle East and Sahara regions, so the dominant tree type in these regions is set as broadleaved deciduous. For pixels in which the tree type – broadleaved or needleleaved, deciduous or evergreen – cannot be assigned based on the neighbourhood window, the majority tree type of the pixel's unique zone is assigned. This method is also applied to assign the types of both shrubs and trees in all shrubland class pixels. Thus, there may be inconsistencies between the shrub type indicated by the class legend and that assigned using this biogeographical approach.

Most of the auxiliary inputs are based on Landsat images and therefore have an extent of 80°N–60°S. The main processing algorithm for the PFT product, explained above for the static pixels, therefore operates on this extent. Less than 0.5 % of the area outside of this extent is composed of pixels belonging to a class other than water bodies (code 210) or permanent snow and ice (code 220). The largest contributors to this small area are the sparse vegetation classes followed by the bare area classes with negligible contributions from shrubland (including flooded shrubland), grassland, and lichens and mosses classes. To extend the PFT product to global extent, the following assumptions are applied to the pixels north of 80°N and south of 60°S: (1) 100 % snow and ice PFT is assigned to pixels of the permanent snow and ice class; (2) 100 % water PFT is assigned to pixels of the water body class; (3) 100 % bare soil PFT is assigned to pixels of the bare area classes; (4) 100 % natural grass PFT is assigned to pixels of the grassland and lichens and mosses classes; (5) 96 % bare soil PFT and 4 % natural grass PFT (to meet the legend minimum of vegetation cover) are assigned to pixels of the sparse vegetation classes; and (6) 84 % natural grass PFT and 16 % needleleaved deciduous shrub PFT (matching the legend minimum shrub cover) are assigned to pixels of the shrubland classes. For the shrubland classes, the shrub type of needleleaved deciduous is assigned because the shrubland class pixels needing assignment (north central Russia) occur nearest pixels of needleleaved deciduous shrubs that had shrub type assigned using the standard method.

### 2.2.2.    Pixels experiencing land cover change

Dynamic pixels – that is, pixels that have experienced at least one land cover class change over the 1992–2020 era – correspond to 5.88 % of the ice-free land surface (Defourny et al., submitted). For such pixels, the derived PFT fractions are derived for each of the classes assigned to that pixel over the era. For example, if a pixel changed from forest to cropland, PFT fractions associated with the forest class are estimated and PFT fractions associated with the cropland class are also estimated for the pixel. The method used to assign the PFT fractions depends on the timestamp of the class in relation to the timestamp (2010) of the auxiliary dataset (Hansen et al., 2013) from which the tree cover fractions are derived. The PFT fraction of a pixel in 2010 was derived using the following class-specific methods described in Sect. 2.2.1. Any change of class occurring before or after 2010 leads to deriving new PFT fractions as the mean PFT fractions of all 300 m pixels of the same class pixels within the overlapping 0.25° x 0.25° window centred on the pixel of interest. The input pixels over which the mean is calculated are the 300 m pixels that did not experience land cover class change over the 1992–2020 era. If no pixels of the relevant class are within the 0.25° x 0.25° window, then the window is incrementally expanded by 0.25° in both the latitude and longitude directions until at least one pixel of the relevant class is contained in the window. A pixel can experience up to 7 land cover changes in the 1992–2020 era (Defourny et al., submitted), which leads to deriving new PFT fractions for each new land cover class encountered.

### 2.3.    Modelling assessment

The impact of the updated PFT distribution on land surface fluxes is evaluated using global simulations of two land surface models: the Organizing Carbon and Hydrology in Dynamic Ecosystems (ORCHIDEE; Krinner et al. 2005 and later revisions) and the Joint UK Land Environment Simulator (JULES; Best et al., 2011; Clark et al., 2011). The simulations with ORCHIDEE focus on evaluating the impact of the updated PFT distributions on a selected set of climate-relevant variables. The ORCHIDEE model applies the Climatic Research Unit (CRU)–Japanese reanalysis (JRA55) v2.0 6-hourly atmospheric driving data for 1901–2018 (Harris et al., 2014; Kobayashi et al., 2015; UEA CRU and Harris, 2019) and the CCI PFT distribution maps for 2010. Two PFT distributions are applied: (1) the new PFT map ($PFT_{local}$) described above and (2) the PFT distribution based on the application of the global standard CWT to the CCI MRLC product for 2010 ($PFT_{global}$) (Table C1) (Hartley et al., 2017, Lurton et al., 2020). The 2010 PFT map is used (recycled) for each year of the simulation. ORCHIDEE is run at a horizontal resolution of 0.5° latitude $\times$ 0.5° longitude over the period 1900 - 2018, and all simulated data before 1980 are discarded as

spin-up, with analysis based on the years 1980–2018. The impact of the updated distribution relative to that based on the global CWT is compared with ORCHIDEE for an ensemble of climate-related variables, including albedo, surface fluxes (latent and sensible heat and their ratio), gross primary productivity, surface temperature, tree fraction, leaf area index (LAI), and above-ground biomass (Sect. 4).

In a separate assessment of the implications of the updated PFT distributions for model evaluation, JULES simulations of PFT distributions, created for the Inter-Sectoral Impacts Model Inter-comparison Project (ISIMIP; Frieler et al., 2017), were used. This was done to compare evaluation results using both the CWT-derived PFT distributions (PFT$_{global}$) and the updated PFT distributions (PFT$_{local}$). The 2010 PFT distributions are used to evaluate the JULES dynamic vegetation results. JULES was driven by the ISIMIP2b protocol described in Frieler et al. (2017) and applied to JULES as described in Mathison et al. (in preparation). Sect. 4.2 describes the Dynamic Global Vegetation Model results for 2010 from the JULES offline simulations driven by HADGEM2-ES climate for the period 1850 to 2100.

## 3.    CCI PFT dataset description

### 3.1.    General description

The CCI PFT dataset (hereafter called PFT$_{local}$) provides the percentage cover as discrete values of 0–100 % of 14 PFTs at 10 arc-second resolution (300 m at the equator; 64,800 pixels in the latitude dimension × 129,600 pixels in the longitude dimension). The global continuous field maps are produced at an annual resolution, covering the years 1992–2020. The PFT distributions are consistent with the CCI MRLC data product and eliminate the need to use a CWT to translate land cover classes into PFTs. The 14 PFTs encompass: (1) permanent inland water bodies; (2) permanent snow and ice cover; (3) bare soil; (4) built-up areas, which includes artificial impervious area such as buildings and, frequently but not exhaustively, other paved surfaces such as roads; (5) managed grasses (i.e., herbaceous crops); (6) natural grasses (i.e., non-cultivated herbaceous vegetation); (7) broadleaved deciduous shrubs; (8) broadleaved evergreen shrubs; (9) needleleaved deciduous shrubs; (10) needleleaved evergreen shrubs; (11) broadleaved deciduous trees; (12) broadleaved evergreen trees; (13) needleleaved deciduous trees; and (14) needleleaved evergreen trees (Figure 1). Following the auxiliary inputs, trees are woody vegetation with a height > 5 m, while shrubs are woody vegetation with a height of 3–5 m, inclusive. An updated water body product (version 4.1) at 150 m resolution, used here to delineate between inland water and ocean, likewise replaces the older version and can be downloaded from the same data repository as the PFT maps.
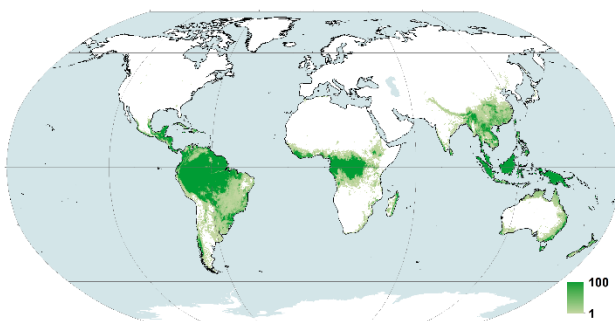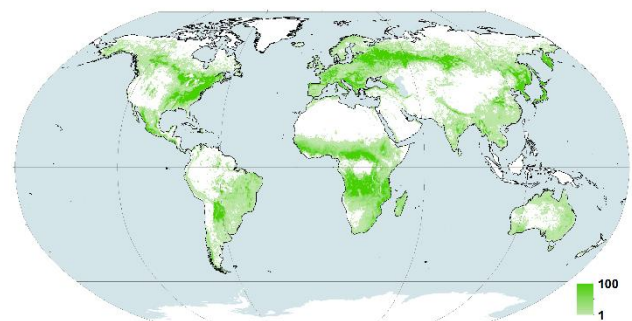


(a)  Broadleaved evergreen trees          (b)  Broadleaved deciduous trees

(c) Needleleaved evergreen trees

(d) Needleleaved deciduous trees

(e) Broadleaved evergreen shrubs

(f) Broadleaved deciduous shrubs

(g) Needleleaved evergreen shrubs

(h) Needleleaved deciduous shrubs

(i) Managed grasses

(j) Natural grasses

(k) Built-up areas

(l) Permanent inland water bodies

(m) Bare soil



(n) Permanent snow and ice cover

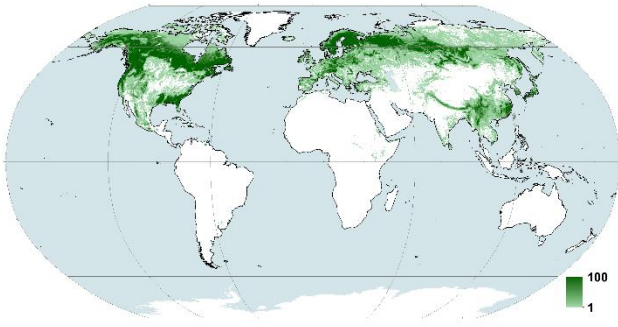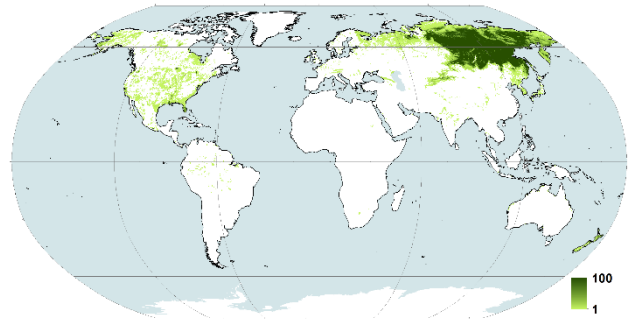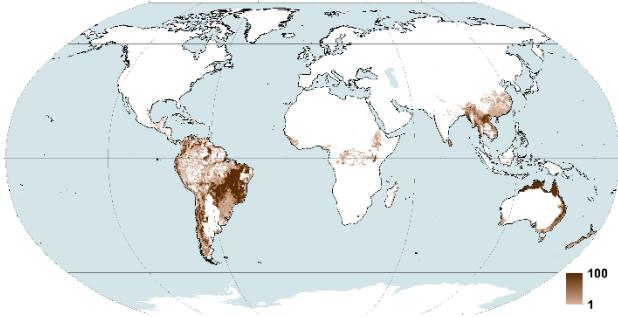**Figure 1. Percentage cover in 2010 for the 14 PFTs included in the** $PFT_{local}$ data product at a spatial resolution of 0.25° × 0.25°. (a) Broad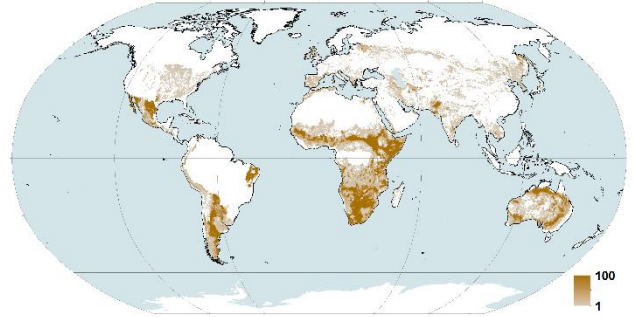leaved evergreen trees, (b) Broadleaved deciduous trees, (c)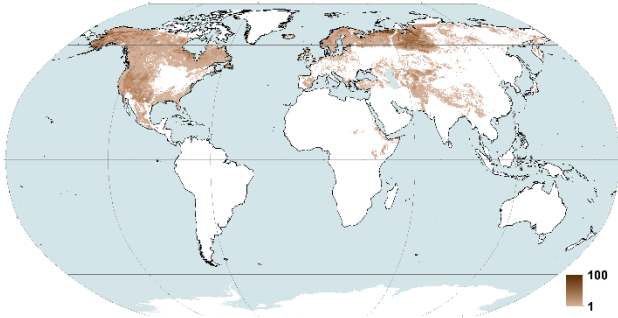 Needleleaved evergreen trees,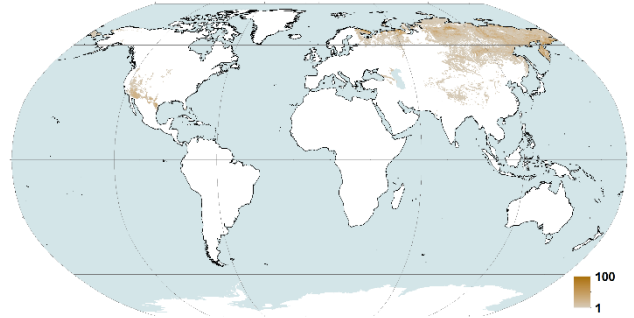 (d) Needleleaved deciduous tr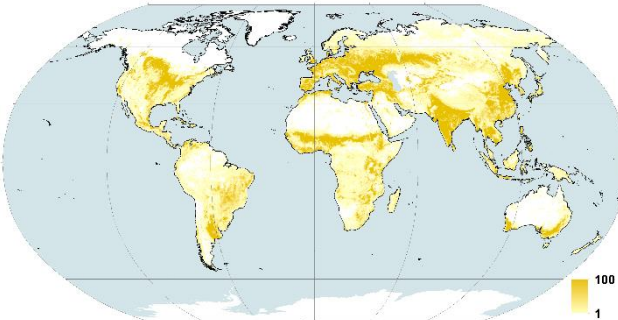ees, (e) Broadleaved evergreen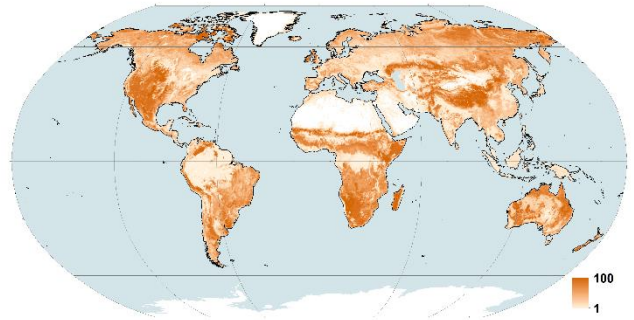 shrubs, (f) Broadleaved decid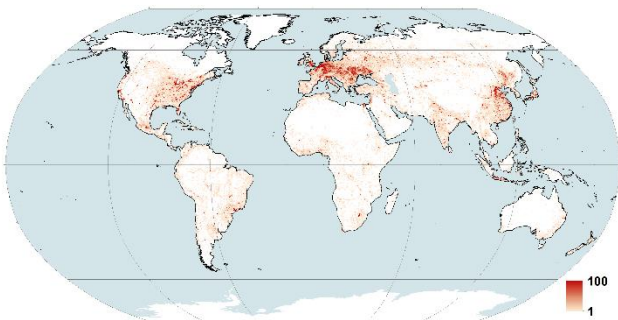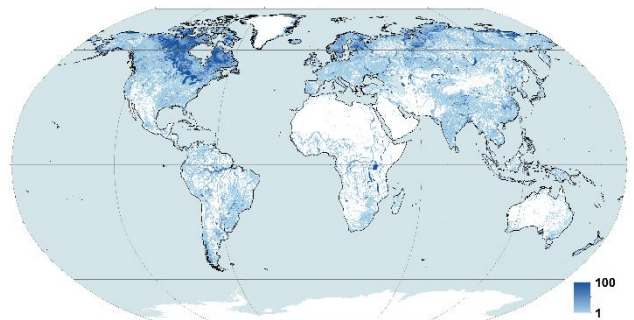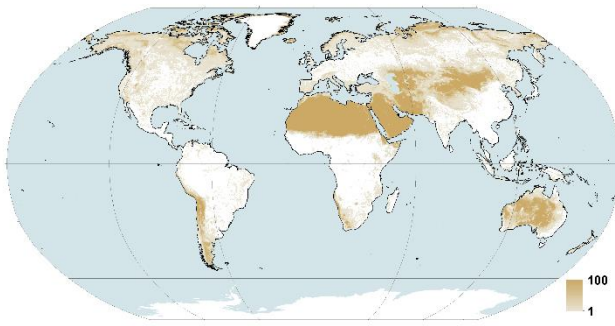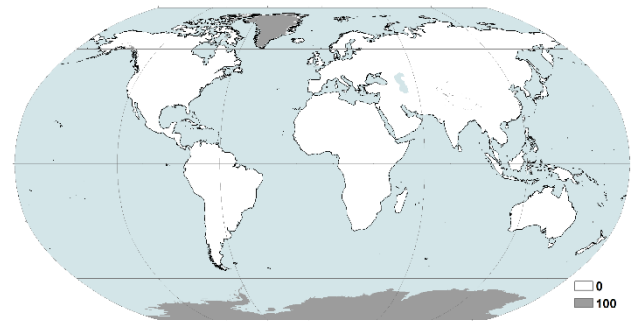uous shrubs, (g) Needleleaved evergreen shrubs, (h) Needleleaved deciduous shrubs, (i) Managed grasses, (j) Natural grasses, (k) Built-up areas, (l) Permanent inland water bodies, (m) Bare soil, and (n) Permanent snow and ice cover.

The $PFT_{local}$ dataset indicates that herbaceous vegetation covers 44.8 % of the Earth's land surface, with around one-third of that area devoted to herbaceous crops. Tree cover accounts for 21.3 % of the land surface, which is much larger than that of shrubs (3.2 %). The abiotic surface types cumulatively cover 30.8 % of the land surface: 18.4 % bare soil, 10.0 % snow and ice, 2.1 % inland water, and 0.3 % built.

The CCI PFT dataset is provided as a companion product to the ESA CCI LC map series products with similar specifications with a global extent, a pixel size of 300 m and a Plate Carrée projection. However, climate models may need products associated with a coarser spatial resolution, over specific areas (e.g., for regional climate models), and/or in another projection. To tackle the variety of requirements, a user tool has been developed that allows users to adjust the products in a way which is suitable to their models. A minimum list of possibilities in terms of spatial resolution and projection has been established and the conversion of CCI-Land Cover classes to other user-defined classes is also foreseen. The CCI PFT product and the user tool are freely available at maps.elie.ucl.ac.be/CCI/viewer/ and climate.esa.int/en/projects/land-cover/data/.

### 3.2.    PFT layer description considering the CCI MRLC categories and the $PFT_{global}$ dataset

Table 3        shows the global areal coverage of each PFT by class for 2010 for the $PFT_{local}$ product, and Table A1 shows the equivalent data corresponding to the application of the most recent version of the CCI MRLC global CWT (Lurton et al. 2020; Table A2) to the v2.0.8 CCI MRLC map for 2010 (hereafter called $PFT_{global}$). Figure A2 complements Table A1 by illustrating the differences between the $PFT_{local}$ and the $PFT_{global}$ products globally at a spatial resolution of 0.25 x 0.25 degrees. For each class of $PFT_{global}$, the global CWT specifies the fractional composition of contributing PFTs; in this approach, each pixel of a class is assigned the same fractional PFT composition regardless of its location on Earth. Table 4      indicates the percentage PFT composition by class for 2010 for $PFT_{local}$, calculated as an area-weighted mean taken over all pixels of the class globally. Figure A3 provides a spatialized summary of the largest differences between the $PFT_{local}$ and the $PFT_{global}$ products. (a) PFTs with the largest increase and (b) corresponding fraction gained, (c) PFT loss and (d) corresponding fractions lost are illustrated globally with 0.25° x 0.25° pixels.

### 3.2.1. Tree cover

The $PFT_{local}$ product indicates global areal tree cover of 31.4 million km$^2$ (Figure 1): 45.2 % broadleaved evergreen; 24.3 % needleleaved evergreen; 23.0 % broadleaved deciduous; and 7.5 % needleleaved deciduous. The PFT $_{local}$ product indicates global areal tree cover that is 4.6 % higher than in the $PFT_{global}$ distribution. Globally, tree coverage is higher in the PFT $_{local}$

14

513     product relative to the $PFT_{global}$ distribution for all tree types except needleleaved deciduous trees. Compared to the global

514     CWT, in which every pixel belonging to a given class is assigned the same PFT fractions, the updated method for estimating

515     PFT fractions locally results in greater variability of tree fractions among 300 m pixels within a single class. For example, the

516     global CWT suggests that all class 10 (rainfed cropland) pixels are 0 % tree cover, but the $PFT_{local}$ product based on auxiliary

517     inputs suggests a much wider range of tree cover at the pixel level, ranging from 0–100 % tree cover at the 300 m pixel level.

518     The distribution for Africa is shown in Figure A1, where tree crops in the Sahel are readily apparent. Globally, class 10 pixels

519     have 5.1 % tree cover on average (Table 4). On average, class 12 pixels (rainfed cropland – tree or shrub cover) have 18.4 %

520     tree cover. The auxiliary dataset used to derive tree cover for most classes in the $PFT_{local}$ product is based on Landsat 7 images

521     (Hansen et al. 2013); the artifacts associated with the failure of the Landsat 7 Scan Line Corrector (Andrefouet et al., 2003)

522     are visible in the 300 m $PFT_{local}$ dataset in some regions, particularly in west-central Africa. Because the PFT product is

523     harmonized with the CCI MRLC class product, potential classification errors can impact the PFT product. For example, recent

524     high-resolution mapping in the circumpolar Arctic (Bartsch et al. 2019) suggests that the CCI MRLC classification may

525     overestimate needleleaved evergreen tree cover in this region, resulting in a possible overestimate of the tree PFT percentage

526     in such pixels. Future improvements to the land cover classification will likewise flow through to the PFT product.


527         **3.2.2. Shrub cover**

528     The $PFT_{local}$ product indicates 4.7 million $km^2$ of global shrub cover. The largest contributors to total shrub cover are

529     broadleaved deciduous (44.6 %) and needleleaved evergreen shrubs (25.2 %). Shrub cover is 74 % lower in the $PFT_{local}$ product

530     than in the $PFT_{global}$ dataset. Some of this difference arises because the $PFT_{local}$ product estimates lower shrub PFT in shrubland

531     class pixels (codes 120–122 and 180) compared to the $PFT_{global}$ dataset, which estimates 8.8 million $km^2$ of shrub PFT in

532     shrubland classes. The area-weighted mean percentage composition of shrubs in shrubland class pixels is 30.0 % for class 120

533     in the $PFT_{local}$ product, 26.1 % for class 121, 34.4 % for class 122, and 30.7 % for class 180. The CWT suggests 60 % shrub

534     cover for classes 120–122 and 40 % for class 180. The CWT estimates 0 $km^2$ of tree PFT cumulatively in these classes

535     compared to 630,000 $km^2$ in the PFT product. The uncertainty associated with the height estimation in the global canopy height

536     product of Potapov et al. (2021) may contribute to the confusion of shrubs and trees in some cases. Nonetheless, the evidence-

537     based $PFT_{local}$ product indicates a significantly lower estimate for global woody vegetation cover in pixels of the shrubland

538     classes compared to the $PFT_{global}$ dataset, which was largely based on expert knowledge.

539

540     In addition to the differences in the shrubland class pixels, a large part of the difference in total shrub cover between the $PFT_{local}$

541     product and the $PFT_{global}$ dataset can be ascribed to the fact that the $PFT_{local}$ product estimates shrub PFT only in pixels

542     belonging to the shrubland classes (codes 120–122 and 180) due to a lack of appropriate datasets to apply to the other classes.

543     The CWT estimates 9.5 million $km^2$ of shrub cover in non-shrubland PFTs, and some of this shrub cover may indeed be

544     missing from the $PFT_{local}$ product. However, because the $PFT_{local}$ product, which is based on quantitative estimation using

545     auxiliary inputs, and the CWT, which is largely based on expert input, differed so strongly in the estimates of shrub PFT in

546     the shrubland class pixels, some of the differences in the non-shrubland class pixels may likewise be due to bias in the CWT.


547         **3.2.3. Natural and managed grasses**

548     Global grass PFT cover in the $PFT_{local}$ product is 65.7 million $km^2$, two-thirds of which is natural grass. Total grass cover is

549     29.6 % higher in the $PFT_{local}$ product than in the $PFT_{global}$ map (38.3 % higher for natural grass and 14.7 % higher for managed

550     grass). In the $PFT_{local}$ product algorithm, for the vegetated classes except for sparse vegetation, the entire non-water fraction

551     of the 300 m pixel is assigned as vegetation; typically, water, trees, and other PFTs are estimated based on auxiliary inputs and

the CCI MRLC class legend, and then the residual area is assigned as grass cover. Thus, grass vegetation may be assigned in some cases that might otherwise be a temporary bare area.

### 3.2.4. Water

In the $PFT_{local}$ product, the per-pixel fraction of surface water PFT is estimated for pixels of all classes except the permanent snow and ice class (**Table 1**). The $PFT_{local}$ product indicates around 142,000 $km^2$ of water cover globally among pixels of all classes except the water body class (code 210). Only two classes – a sparse vegetation sub-class (code 151) and a needleleaved deciduous tree cover sub-class (code 82) – have no pixels with inland water cover (Table 3    ), but both classes have extremely limited total areal coverage, each accounting for only a few square kilometres of area globally. Classes with significant water coverage include: needleleaved evergreen tree cover classes 70 and 71 (40,000 $km^2$ combined); sparse vegetation class 150 (20,000 $km^2$); lichens and mosses class 140 (14,000 $km^2$); flooded shrub/herbaceous cover class 180 (12,000 $km^2$); and bare area class 200 (12,000 $km^2$). Coverage of water PFT in pixels of the non-water body classes is especially prevalent in the boreal region. Classes with the highest fractional composition of inland water – calculated as the area-weighted mean among all pixels of the class globally (Table 4) – include the flooded tree cover class 170 (2.3 %), the needleleaved evergreen tree cover class 72 (1.3 %), and the lichens and mosses class 140 (0.9 %).

The $PFT_{local}$ product indicates 3 % (91,000 $km^2$) lower inland water fractional cover than the $PFT_{global}$ product distribution. While the non-water body classes have a total inland water PFT cover of 142,000 $km^2$ in the $PFT_{local}$ product (compared to 0 $km^2$ from the $PFT_{global}$), the $PFT_{local}$ product indicates a lower inland water PFT area in the water body class than does the CWT (difference of 233,000 $km^2$). The difference in the water body class occurs because the $PFT_{local}$ product allows up to 14 % vegetation cover in this class whereas the CWT assumes 100 % water PFT. PFTs with significant global coverage in water body class pixels in the $PFT_{local}$ product include natural grasses (183,000 $km^2$) and needleleaved evergreen trees (31,000 $km^2$) with smaller contributions from the other tree types.

### 3.2.5. Bare

In the $PFT_{local}$ product, bare soil PFT occurs in the bare area classes (codes 200–202) and the sparse vegetation classes (codes 150–153), accounting for 19.4 million $km^2$ and 7.6 million $km^2$ bare soil area, respectively, at the global scale (Table 3). The global area-weighted mean bare soil percentages are 85.9 % in sparse vegetation class pixels and 99.9 % in bare area class pixels, which are nearly identical to the compositions suggested by the global CWT (85 % for sparse vegetation classes and 100 % for bare area classes). Cumulatively for these classes, the $PFT_{local}$ product suggests only 0.2 % lower bare soil PFT coverage at the global scale relative to the assumed distribution in the $PFT_{global}$ dataset (difference of 65,000 $km^2$). In the $PFT_{local}$ product, the bare area classes contain, in addition to bare soil PFT, inland water PFT (13,000 $km^2$) and tree cover (1,000 $km^2$).

The $PFT_{local}$ product does not include bare soil PFT in the shrubland classes, while the $PFT_{global}$ dataset assumes 20 % bare soil for the non-flooded shrubland classes 120–122. Because the non-flooded shrubland class pixels have such a large extent globally (13.3 million $km^2$), the $PFT_{global}$ dataset suggests 2.7 million $km^2$ of additional bare soil in such pixels relative to the PFT product. Differences in the distribution of bare area between the $PFT_{local}$ product and the $PFT_{global}$ product are especially pronounced in the U.S. intermountain west, parts of southern and eastern Africa, the northern coast of Australia, and the highlands of Argentina and Brazil, as these are regions with significant shrubland class cover. In the $PFT_{local}$ product, all residual area in the shrubland class pixels that is not assigned as surface water or woody vegetation (trees and/or shrubs) based on the auxiliary input data is assigned as natural grass cover rather than bare soil.

In the PFT $_{local}$ product, the bare soil PFT represents areas that are not expected to support vegetation regardless of environmental conditions. For shrubland class pixels, we assume that vegetation growth can be supported given the appropriate environmental conditions; therefore, the residual pixel area (after accounting for inland water, tree, and shrub cover) is assigned as natural grass PFT. Since the PFT $_{local}$ product is built mainly for application to land surface models, the actual presence of grass vegetation vs. bare soil for such pixels (of the shrubland class, but also of the other vegetated classes) will be determined by the model given simulated or prescribed local climate conditions. Users should consider the definition of the bare soil PFT to determine suitability of the data product for their use case.

### 3.2.6. Built fraction

Both the PFT$_{local}$ product and the PFT$_{global}$ assign built PFT only to pixels of the urban class (code 190). The presence of a built PFT is not universal in land surface or Earth system models; for example, the current version of the ORCHIDEE land-surface model considers built areas to be 80 % bare soil and 20 % grasslands. The cross-walking of land cover classes to PFTs for the urban class strongly depends on the framework used to calculate surface fluxes in the urban environment and therefore inter-model variation in the global CWT may be stronger for the urban class than for vegetated classes. The global CWT used for this analysis assigns 100 % of the urban class as built PFT. For comparison, the JULES land surface model assigns urban class pixels as 75 % built and 25 % bare soil.

The PFT$_{local}$ product suggests 477,000 km$^2$ of built area globally (Table 3), which corresponds to an area-weighted mean composition of 73.7 % built PFT in urban class pixels (Table 4). The auxiliary inputs suggest that about 1.6 % of urban class pixels have 0 % built PFT coverage. This suggests a mismatch between the land cover classification and the auxiliary inputs for a small number of pixels, which could be related to a mismatch in the time stamp of the auxiliary inputs (2014) relative to the land cover dataset. Considering all urban class pixels, 6.2 % have built PFT of 0–25 %, 7.8 % have built PFT of 26–50 %, 31.9 % have built PFT of 51–75 %, and 54.1 % have built PFT of 76–100 %. As area-weighted means, the non-built portion of urban class pixels is 25.1 % natural grass cover, 0.3 % inland water, and 0.9 % tree cover. The increased spatial heterogeneity in urban class pixels due to the PFT$_{local}$ product is readily apparent in Figure 2, which shows the PFT distribution for Amsterdam, the Netherlands. The more realistic characterization of the urban environment in the PFT$_{local}$ product that gives more variability of built PFT coverage within a city should allow a more faithful representation of urban surface fluxes in land-surface models.
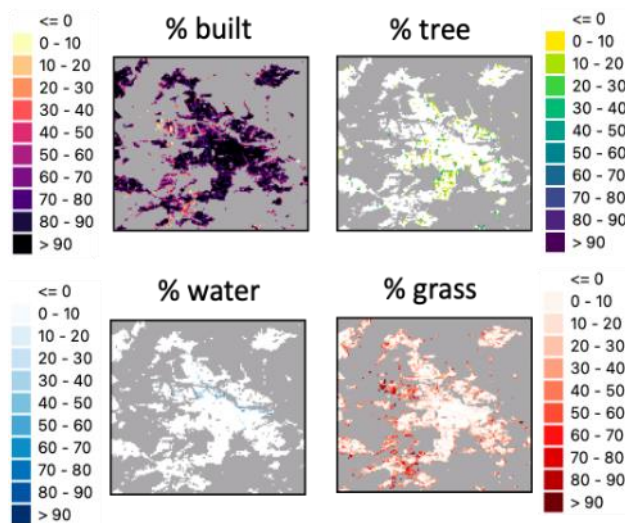


**Figure 2.** Percentage cover in 2010 for built, total tree, grass, and inland water PFTs in Amsterdam, the Netherlands, in the PFT$_{local}$ product.

### 3.2.7. Permanent snow and ice

624 The permanent snow and ice in PFT$_{local}$ accounts for 14.7 million km$^2$ of area globally, largely in Greenland and Antarctica,

625 but also in the Arctic and mountainous regions of Asia. The PFT$_{local}$ product and PFT$_{global}$ dataset indicate identical coverage

626 for this PFT since both datasets assign 100 % snow and ice PFT to the permanent snow and ice class (code 220) and 0 % snow

627 and ice PFT to all other classes.

### *4.* **Modelling results**

### 4.1. **ORCHIDEE simulations: new PFT product (PFT$_{local}$) vs PFT maps based on global CWT (PFT$_{global}$)**
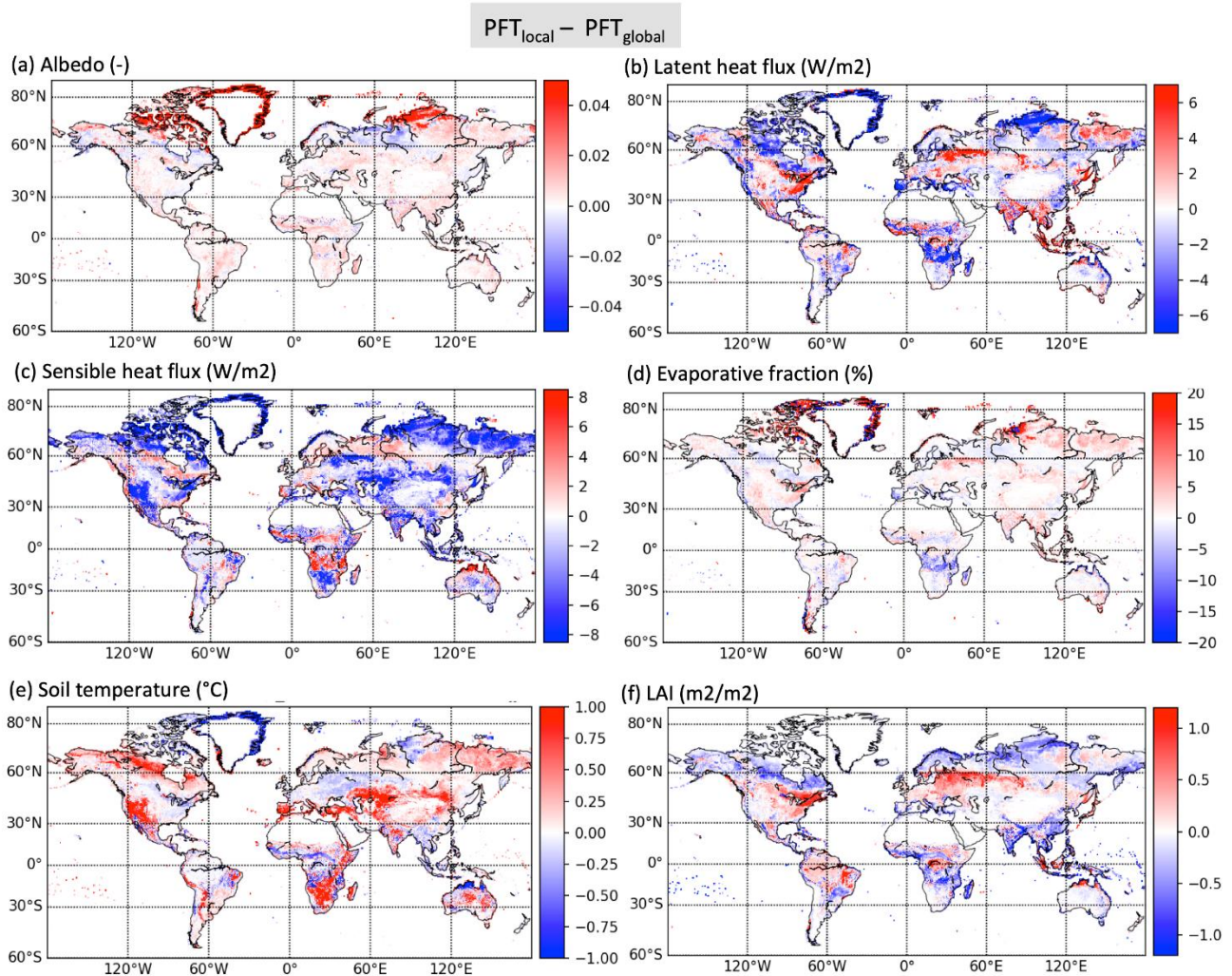


**Figure 3.** Differences in (a) albedo, (b) latent heat flux, (c) sensible heat flux, (d) evaporative fraction (Latent heat flux / (Latent + Sensible heat fluxes), (e) soil surface temperature, and (f) Leaf Area Index (LAI) simulated by the ORCHIDEE model between the new PFT (PFT$_{local}$) and the old PFT distributions (PFT$_{global}$), for the summer (June - July - August, northern hemisphere) of year 2010.

634 In this section, we compare the results of two ORCHIDEE simulations performed, respectively, by applying the old standard

635 PFT maps (PFT$_{global}$) and the new PFT product derived in this study (PFT$_{local}$). The results are shown for the year 2010.

636 The impacts of the changes in the land surface representation between the local and global PFT maps on the surface albedo,

637 latent and sensible heat fluxes, evaporative fraction (ratio of latent heat flux to the sum of latent and sensible heat fluxes),

638 surface temperature, and the LAI are shown in Figure 3. Averaged differences (local vs global) for the northern hemisphere

639 summer period (June-July-August, JJA) were plotted here to highlight the main changes but the plots at the annual scale are

640 also given in the Supplementary Information. The results show that the energy, water, and carbon fluxes are mainly (and

641 significantly) impacted in the regions where woody vegetation was replaced by grasslands or where the bare soil fraction has

18

changed. Since, in ORCHIDEE, the shrub PFTs are assigned to tree PFTs, the regions highlighted in Sect. 3 with significant fractions of shrub losses or gains in profit of grasses show the largest changes. Given that tree PFTs present a lower albedo, higher roughness (linked to vegetation height) and maximum transpiration capacity, and higher LAI and biomass, the simulated differences between the two simulations show coherent features across the different variables. In summer, surface albedo increases up to 4 % (absolute deviation) in the northern boreal regions because of the decrease of shrubs and the increase of grasslands and in some regions (like in the Taymir peninsula) the increase of bare soils. More southern of this boreal zone, both in Eurasia and North America, the increase of trees and decrease of shrubs, show opposite variations. In the tropical region (between 0° and 30°S), the PFT changes principally concern differences in the shrubs/grasses partition at the benefit of grasslands. In these regions, the tree fraction decrease results in a slight increase of the albedo around 2 % (absolute deviation). At the annual scale (Figure B1), the larger impact of the PFT differences in the high latitudes is explained by the cumulative impact of changes in snow cover. Indeed, snow melting is more rapid on tree cover compared to grasslands, inducing a shorter duration of the snow cover with high albedo values, leading to even more differences between short and high vegetation albedo values.

Surface albedo differences (impacting surface net radiation) combined with roughness changes (impacting turbulent exchanges) explain generally the surface flux variations. The balance between the two effects varies according to the latitude following the amount of solar radiation: in the northern latitudes, the impact of surface roughness is larger than in more southern ones. In the tropics, we observe a decrease in the turbulent fluxes where the albedo is larger, explaining the lower evapotranspiration and lower GPP, with different partitions when comparing arid and humid zones. For example, the consequences of a decrease of shrubs to the benefit of grasses do not have the same effects on the heat flux partition according to the water availability. In regions where soil moisture limits evapotranspiration, like central Africa (south of the Democratic Republic of the Congo) or the Sahel, fewer trees lead to less evapotranspiration up to 6 $Wm^{-2}$ in annual mean, and larger sensible heat flux at the same level, whereas in the northern latitudes like in eastern Siberia, fewer shrubs lead to larger evapotranspiration and lower sensible heat flux. This is summarized in the representation of the evaporative fraction which shows opposite variations in these regions.

The surface temperature, as the result of the energy and water budgets, shows differences in line with the sensible heat flux variations, with larger temperatures where the sensible heat flux has decreased. The differences in summer and in annual mean are significant and can reach 1 K but can show differences up to 3 K on a daily scale.

LAI differences are in coherence with the PFT differences: lower values where woody vegetation was replaced by grasses, except in eastern Siberia and northern Australia where the increase of net radiation favored transpiration and GPP and, finally, LAI. The LAI variations may reach 1 $m^2m^{-2}$ in some regions like southeastern Canada or Central Europe, where the broadleaf deciduous trees have increased in the $PFT_{local}$ map.

Figure 4 illustrates the impacts on the above-ground biomass (AGB) with the tree cover variations. To see if the biomass changes are more realistic, they have been compared to the ESA CCI Biomass product, version 3 ($ESA_{CCI}$ Biomass, Santoro and Cartus, 2019; Santoro et al., 2021) aggregated at 0.5° resolution. Note that, unlike for the turbulent fluxes discussed above, the change in AGB between low and high vegetation covers should be large enough and thus easier to evaluate. In Figure 4ab, we first compare the simulated AGB with the new PFTs ($PFT_{local}$) to the $ESA_{CCI}$ Biomass product, which highlights some issues related to ORCHIDEE model deficiencies and also, in part, to relatively large errors in the $ESA_{CCI}$ Biomass product, especially for high AGB. -The model simulates too low AGB on average with a large underestimation over the tropical forests, which cannot be due to the PFT cover (above 90 % forest cover). Over temperate and high latitudes, we also find significant

model AGB underestimation. The improvements/degradations with respect to changing the PFT distribution (Figure 4d; where the mean errors between the two simulations performed with $PFT_{local}$ and $PFT_{global}$ are represented), provide contrasting results between regions. The benefits of the new $PFT_{local}$ maps (blue color in Figure 4d) are visible in northeast Europe, the eastern USA and in Democratic Republic of the Congo where the increase of tree fraction (Figure 4c) and biomass seems to be in better agreement with the remote sensing AGB product. In the other regions, where the tree fractions decreased (northern Canada and Europe, Sahel, Angola, Zambia and southern China, Figure 4c), the associated decrease of biomass leads to larger errors compared to the AGB satellite product. In the western USA (California), the losses of tree PFTs to the benefit of grasslands did not impact the simulated biomass since, in these arid regions, the trees have very low productivity comparable to grasses and thus similar low biomass values (less than 1 KgCm$^{-2}$).

Overall, these results highlight the importance and impact of land surface PFT distribution on simulated energy, water, and carbon fluxes as well as carbon stocks in global land surface models.
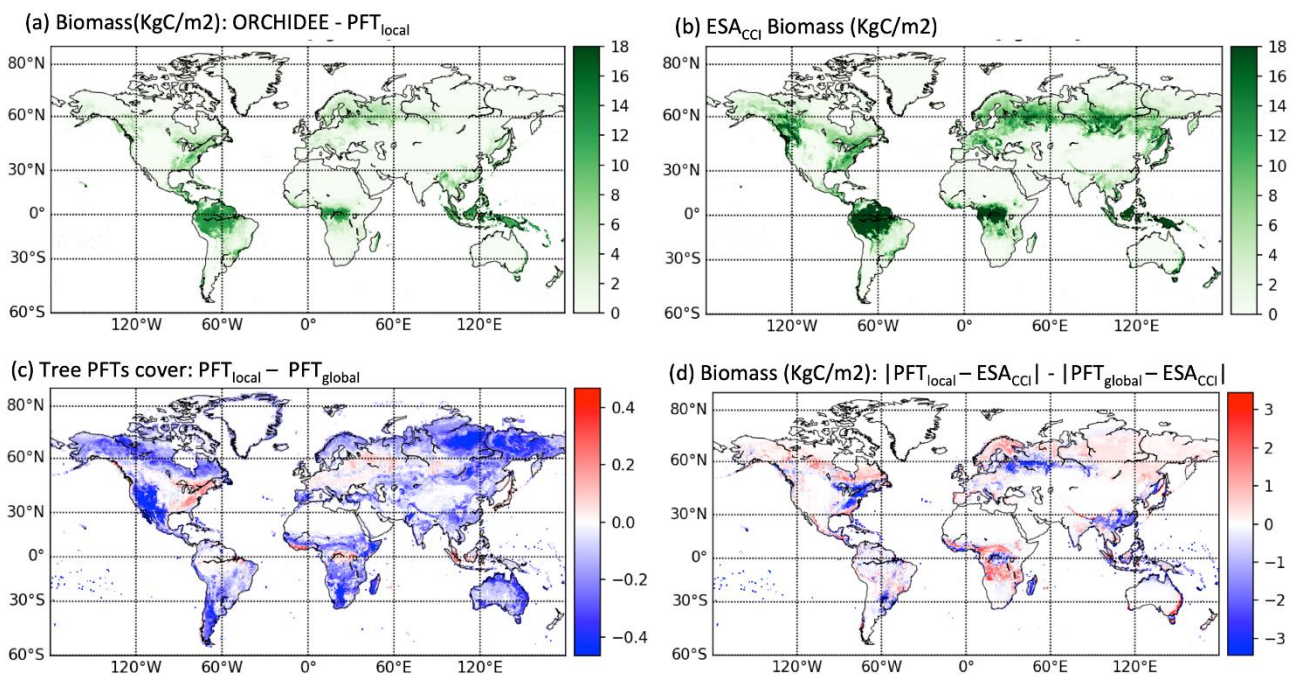


**Figure 4.** Above Ground Biomass (AGB) (a) simulated by the ORCHIDEE model with the $PFT_{local}$ dataset and (b) observed by the $ESA_{CCI}$ Biomass product version v3, for the year 2010 (Santoro and Cartus (2019)); (c) Differences in the tree PFT fraction prescribed; (d) Difference between the mean bias of simulated versus $ESA_{CCI}$ Biomass AGB between the new ($PFT_{local}$) and the former ($PFT_{global}$) distributions of PFTs. Negative values indicate a decrease in the bias from the $PFT_{global}$ to the $PFT_{local}$.

## 4.2. Evaluation of DGVM (JULES-TRIFFID) using PFT fractions

The impact of using the new PFT distributions ($PFT_{local}$) as a benchmark for JULES-TRIFFID dynamic vegetation is shown in Figure 5. In contrast to results shown in Sect. 4.1, differences found here indicate the value of the new PFT distributions as a product for model evaluation, rather than a direct improvement of model predictions. When compared to $PFT_{global}$ ('CWT'), JULES-TRIFFID indicates significant over-estimation of tree cover in tropical savannahs, and under-estimation of tree cover in boreal northeast Russia. Additionally, comparison with the global CWT product ($PFT_{global}$) indicates that JULES-TRIFFID under-estimates shrub cover in tropical savannas in South America, Africa, and Australia, as well as many semi-arid regions such as western North America. Biases in grass cover are more spatially heterogeneous, but comparison with the global CWT indicates that JULES-TRIFFID strongly over-estimates in northeast Russia and northern Australia.

When using the new PFT distributions as a benchmark, many of these biases are reduced, as indicated by green areas in column "c" of Figure 5. In particular, northeast boreal Russia shows reduced biases in tree, shrub, and grass cover. Globally, using the new PFT distributions results in a reduction in biases in shrub cover in JULES-TRIFFID in almost every part of the world, particularly savannahs and semi-arid regions (Figure 4d). Whilst no large areas showed a large increase in bias, some areas did show increases in bias of up to 25 %, such as tropical forests (10 % increase), grass cover in tropical savannahs (15 to 25 %) and northern high latitudes (10 to 20 %), and bare cover in arid regions (up to 10 % increase).
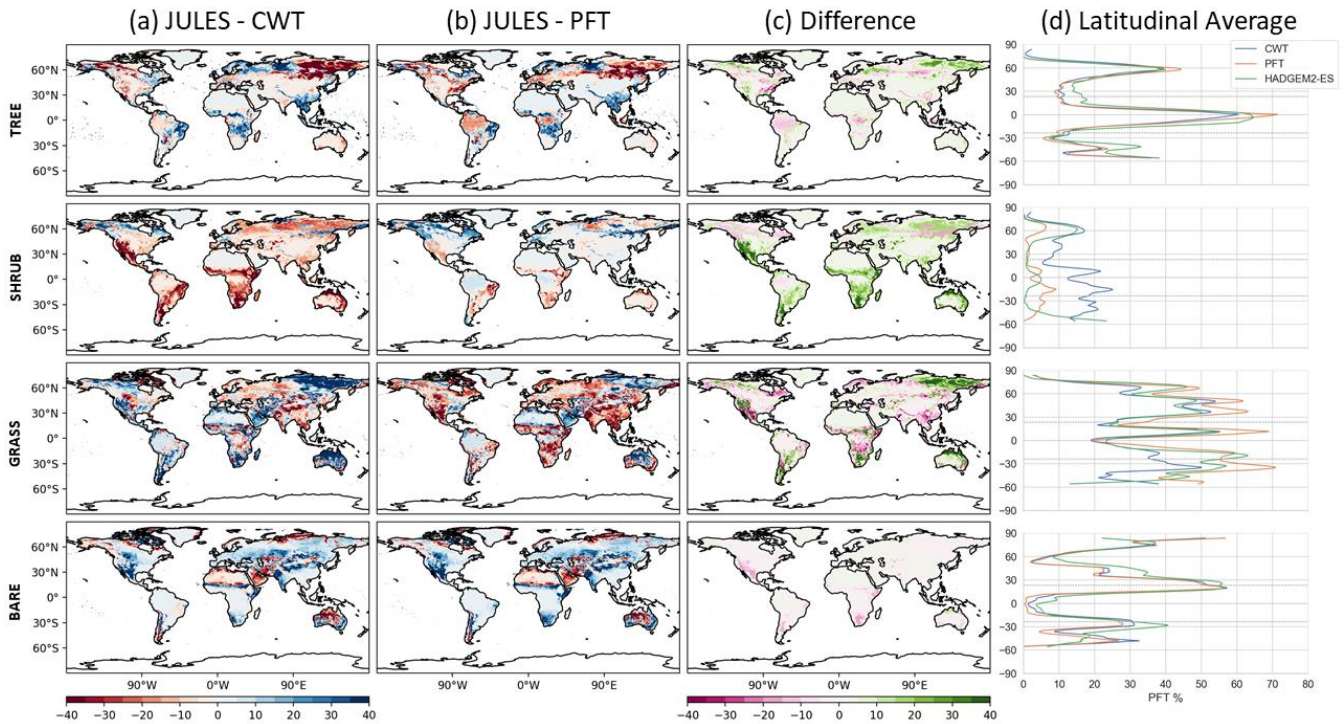


**Figure 5.** Comparison of JULES PFT distributions to both the CWT (PFT$_{global}$) and PFT (PFT$_{local}$) products for major vegetation types. Rows show each major surface type (Tree, Shrub, Grass, Bare), whilst rows show (a) JULES vegetation distribution compared to the global CWT; (b) the same compared to new PFTl$_{local}$ distributions; (c) the difference between (a) and (b), where green (pink) indicates positive or negative anomalies evaluate closer to 0 (further away from 0) using new PFT$_{local}$ distributions; (d) absolute latitudinal average fractions for each major vegetation type from CWT, PFT, and JULES.

## 5. Conclusion and perspectives

The new PFT product (PFT$_{local}$) was generated to reduce the cross-walking component of uncertainty by adding spatial variability to the PFT composition within a LC class. This work moved beyond fine-tuning the cross-walking approach for specific LC classes or regions and, instead, separately quantifies the PFT fractional composition for each 300 m pixel globally. The result is a dataset representing the cover fractions of 14 PFTs at 300 m for each year in the 1992–2020 era, consistent with the CCI MRLC map for the corresponding year. The PFT$_{local}$ dataset exhibits intraclass spatial variability in PFT fractional cover at the 300 m pixel level and is complementary to the CCI medium resolution multi-mission LC map series since the derived PFT fractions maintain consistency with the original LC class legend.

The PFT$_{local}$ dataset provides a more faithful representation of PFT distributions because it draws on high-resolution peer-reviewed mapping of specific vegetation classes to refine global assumptions about PFT fractions. In many cases, the global CWT presented a reasonable approximation for estimating PFT fractions within many land cover classes as shown by the fractions estimated from the auxiliary products falling close to that suggested by the global CWT.

Note that a recent study by Marie et al. (2022) followed the same objective of refining the global CWT (used to map the ESA land cover classes onto PFTs) but with a different approach. Instead of using the tree cover dataset from Hansen et al. (2013), they valorised a map of above-ground biomass over Africa (Bouvet et al., 2018) to define local CWTs, using the information from AGB to better constrain the partition between tree and short vegetation PFTs, for each LC class. As shown in our study, they found that LC class 10 (rainfed cropland) in the Sahel should contain tree PFTs which correspond to tree crops (Figure A1). Overall, these efforts highlight the benefits of using additional high-resolution products, like tree cover, AGB, etc. when translating land cover into PFT distributions for land surface models. Merging all sources of information into a coherent PFT product remained however a difficult task. This study demonstrated that using the consistent CCI MRLC time series and maintaining deference to the original LCCS class in the combination rules allowed bringing these auxiliary data into consistency.

Changing the PFT distribution in the ORCHIDEE model ($PFT_{local}$ vs $PFT_{global}$) induces significant impacts on the simulated water, energy, and carbon fluxes as well as on the modelled carbon stocks. These differences are coherent with changes in surface properties (albedo, roughness, type of cover) induced by changes in PFT types (mainly tree vs short vegetation and bare soil covers). However, it is not possible and beyond the scope of the paper to evaluate globally and quantitatively model improvements due to changes in PFTs given i) existing model biases that have been partly compensated by previous model parameters tuning with the old PFT maps ($PFT_{global}$) and ii) the large uncertainty still associated with data-driven products at global scale. We initiated an evaluation with AGB; however, the new simulated biomass (induced by PFT changes) is not always closer to the satellite $ESA_{CCI}$ AGB product. In addition, the fact that ORCHIDEE does not differentiate shrubs and trees limits such biomass evaluation. Additional simulations/tests with more models and a more comprehensive evaluation with a larger ensemble of variables and data-driven products are therefore needed to quantify the benefits of the $PFT_{local}$ maps.

Using the $PFT_{local}$ as a benchmark improves the evaluation of every major surface type in the JULES-TRIFFID dynamic vegetation model, particularly shrub cover. This allows a new perspective on priorities for dynamic vegetation model development.

The user tool described in Poulter et al. (2015) has been reformatted such that it can be applied directly to the new PFT map series to create user-specific ready-to-use inputs for LSMs. The user tool creates model-ready inputs at user specification, which greatly expands the ease of use of the product both within and beyond the modelling community. The PFT dataset is designed primarily for use in land surface and Earth system models. For the vegetated classes except for sparse vegetation, the entire non-water fraction of the 300 m pixel is assigned as vegetation, allowing the actual presence of grass vegetation to be determined by the land surface models. For use outside of modelling, this could introduce some bias (e.g., underestimating bare soil cover in some pixels and overestimating grass cover), but the fractions of the high biomass veg types (trees and shrubs) can be used for non-modelling use cases.

Production of the $PFT_{local}$ product is dependent on the availability and quality of the auxiliary datasets at a spatial resolution higher than 300 m; this is especially critical for mapping the shrubland class. With the combined information of the phenological attribute of the ESA CCI LC classes, the percentage of tree canopy cover from Hansen et al. (2013), and the GEDI product (Potapov et al., 2021), it was possible, for the first time, to map four shrubland classes at the global scale: broadleaved evergreen, broadleaved deciduous, needleleaved evergreen, and needleleaved deciduous. Yet, further research is still needed to improve the estimation of shrubland class pixels north of 52°N (i.e., outside of the extent of the GEDI product). The urban PFT would benefit from separating impervious surfaces from buildings. Finally, the current workflow should further

be tested against annual ancillary product updates as operational production of very-high-resolution datasets becomes the norm.

The proposed methodology is automated so that the PFT dataset will be updated annually as new annual land cover maps are produced in C3S. Because the PFT product is harmonized with the CCI MRLC map series, future improvements in the land cover product will flow through to the PFT product.

Tables

**Table 1.** For each of the 22 global and 15 regional land cover classes of the CCI MRLC map series, listed are the set of contributing PFTs with the possibility for non-zero fractional cover. The regional land cover classes with codes ending with 1, 2, or 3, are thematically richer than the global classes but can be found only at the regional scale depending on training data availability.

| Class code | Class description | PFTs for which non-zero fractions are permitted in the PFT product |
|---|---|---|
| 10 | Rainfed cropland | Trees, water, managed grass |
| 11 | Rainfed cropland – herbaceous cover | Trees, water, managed grass |
| 12 | Rainfed cropland – tree or shrub cover | Trees, water, managed grass |
| 20 | Irrigated or post-flooding cropland | Trees, water, managed grass |
| 30 | Mosaic: > 50 % cropland/ < 50 % natural tree, shrub, herbaceous cover | Trees, water, managed grass |
| 40 | Mosaic: > 50 % natural tree, shrub, herbaceous cover/ < 50 % cropland | Trees, water, natural grass, managed grass |
| 50 | > 15 % broadleaved evergreen tree cover | Broadleaved evergreen trees, water, natural grass |
| 60 | > 15 % broadleaved deciduous tree cover | Broadleaved deciduous trees, water, natural grass |
| 61 | > 40 % broadleaved deciduous tree cover | Broadleaved deciduous trees, water, natural grass |
| 62 | 15–40 % broadleaved deciduous tree cover | Broadleaved deciduous trees, water, natural grass |
| 70 | > 15 % needleleaved evergreen tree cover | Needleleaved evergreen trees, water, natural grass |
| 71 | > 40 % needleleaved evergreen tree cover | Needleleaved evergreen trees, water, natural grass |
| 72 | 15–40 % needleleaved evergreen tree cover | Needleleaved evergreen trees, water, natural grass |
| 80 | > 15 % needleleaved deciduous tree cover | Needleleaved deciduous trees, water, natural grass |
| 81 | > 40 % needleleaved deciduous tree cover | Needleleaved deciduous trees, water, natural grass |
| 82 | 15–40 % needleleaved deciduous tree cover | Needleleaved deciduous trees, water, natural grass |
| 90 | Mixed leaf type (broadleaved and needleleaved) tree cover | Trees, water, natural grass |
| 100 | Mosaic: > 50 % tree and shrub cover / < 50 % herbaceous cover | Trees, water, natural grass |
| 110 | Mosaic: > 50 % herbaceous cover / < 50 % tree and shrub cover | Trees, water, natural grass |
| 120 | Shrubland | Trees, water, natural grass, shrubs |
| 121 | Evergreen shrubland | Trees, water, natural grass, shrubs |
| 122 | Deciduous shrubland | Trees, water, natural grass, shrubs |
| 130 | Grassland | Trees, water, natural grass |
| 140 | Lichens and mosses | Water, natural grass |
| 150 | Sparse vegetation: < 15 % tree, shrub, herbaceous cover | Trees, water, natural grass, bare soil |
| 151 | Sparse vegetation: < 15 % tree cover | Trees, water, natural grass, bare soil |
| 152 | Sparse vegetation: < 15 % shrub cover | Trees, water, natural grass, bare soil |
| 153 | Sparse vegetation: < 15 % herbaceous cover | Trees, water, natural grass, bare soil |
| 160 | Flooded tree cover – fresh or brackish water | Trees, water, natural grass |
| 170 | Flooded tree cover – saline water | Trees, water, natural grass |

| | | |
|---|---|---|
| 180 | Flooded shrub or herbaceous cover – fresh, saline, or brackish water | Trees, water, natural grass, shrubs |
| 190 | Urban areas | Trees, water, natural grass, built |
| 200 | Bare areas (total vegetative cover < 4%) | Trees, water, bare soil |
| 201 | Consolidated bare areas | Trees, water, bare soil |
| 202 | Unconsolidated bare areas | Trees, water, bare soil |
| 210 | Water body | Trees, water, natural grass |
| 220 | Permanent snow and ice | Snow and ice |

793

794 Table 2. Summary of method applied to derive pixel-level functional type composition by land cover class. See Table 1 for
795 more comprehensive class descriptions. PEA16 = surface water data product of Pekel et al. 2016. HEA13 = tree canopy cover
796 product of Hansen et al. 2013. PEA13 = Global Human Settlement Layer from Pesaresi et al. 2013. PEA21 = tree canopy
797 height dataset of Potapov et al. 2021. For the calculation of tree percentage: "Method 1" indicates that, in cases of disagreement
798 in tree cover percentage between the ancillary dataset and the class legend, a window of up to 0.5° x 0.5° is used to estimate the
799 final tree cover percentage based on neighborhood pixels of the same class; and "Method 3" indicates that an upper limit of 14
800 % tree cover is applied based on the class definition. See the text for additional details about the processing and use of the
801 ancillary data products, the method used to align the derived PFT percentages with the class legend, the scaling method applied
802 in cases where the sum of PFT percentages from the ancillary data exceeds 100% in a pixel, and the method used to derive the
803 PFT fractional composition for pixels falling outside of the extents of the ancillary datasets.

| Class description | Inland water % | Tree % | Tree type | Grass % | Grass type | Shrub % | Bare soil % | Built % | Snow/ice % |
|---|---|---|---|---|---|---|---|---|---|
| Rainfed cropland (10-12) | PEA16 | HEA13 | Neighborhood majority | 100% - water % - tree % | Managed | 0% | 0% | 0% | 0% |
| Irrigated or post-flooding cropland (20) | | | | | | | | | |
| Mosaic of cropland and natural vegetation (30) | | | | | | | | | |
| Mosaic of cropland and natural vegetation (40) | | | | | Managed & natural mixture | | | | |
| Mosaic of tree/shrub and herbaceous (100 & 110) | | | | | Natural | | | | |
| Grassland (130) | | | | | | | | | |
| Broadleaved evergreen tree cover (50) | | HEA13, Method 1 | Class legend | | | | | | |
| Broadleaved deciduous tree cover (60-62) | | | | | | | | | |

| | | | | | | | | |
|---|---|---|---|---|---|---|---|---|
| Needleleaved evergreen tree cover (70-72) | | | | | | | | |
| Needleleaved deciduous tree cover (80-82) | | | | | | | | |
| Mixed leaf type tree cover (90) | | | Neighborhood majority | | | | | |
| Flooded tree cover (160-170) | | | | | | | | |
| Lichens and mosses (140) | | 0% | N/A | 100% - water % | | | | |
| Sparse vegetation (150-153) | | HEA13, Method 2 | Neighborhood majority | Tree % + grass % must be in range 4-14% | | | 100% - water % - tree % - grass % | |
| Shrubland (120-122) | | PEA21 | Biogeographical approach | 100% - water % - tree % - shrub % | | PEA21 | 0% | |
| Flooded shrub or herbaceous cover (180) | | | | | | | | |
| Urban areas (190) | | HEA13 | Neighborhood majority | 100% - water % - tree % - built % | | 0% | | PEA16 |
| Bare areas (200-202) | | | | 0% | N/A | | 100% - water % - tree % | 0% |
| Inland water bodies (210) | | | | 100% - water % - tree % | Natural | | 0% | |
| Ocean (210) | 100% | 0% | N/A | 0% | N/A | | | |
| Permanent snow and ice (220) | 0% | | | | | | | 100% |

804

805

**Table 3.** Global areal cover (1000 km²) of each PFT by land cover class for 2010 in the PFT$_{local}$ product.

| Class | Bare soil | Built | Managed grasses | Natural grasses | Snow/ice | Water[1] | BD trees | BE trees | ND trees | NE trees | BD shrubs | BE shrubs | ND shrubs | NE shrubs |
|---|---|---|---|---|---|---|---|---|---|---|---|---|---|---|
| 10 | 0 | 0 | 7729.7 | 0 | 0 | 2.3 | 175.1 | 199.5 | 0.7 | 36 | 0 | 0 | 0 | 0 |
| 11 | 0 | 0 | 6774.9 | 0 | 0 | 1.5 | 110.4 | 112.9 | 4.1 | 19.7 | 0 | 0 | 0 | 0 |
| 12 | 0 | 0 | 155.1 | 0 | 0 | 0.1 | 4.6 | 29.8 | 0 | 0.6 | 0 | 0 | 0 | 0 |
| 20 | 0 | 0 | 2415.5 | 0 | 0 | 1.2 | 19 | 7.4 | 0.2 | 1.8 | 0 | 0 | 0 | 0 |
| 30 | 0 | 0 | 2803 | 0 | 0 | 1.1 | 123.2 | 467.2 | 0.8 | 39 | 0 | 0 | 0 | 0 |
| 40 | 0 | 0 | 1557.4 | 1247.9 | 0 | 1.2 | 195.1 | 493.2 | 4.7 | 65.1 | 0 | 0 | 0 | 0 |
| 50 | 0 | 0 | 0 | 1262.6 | 0 | 4.3 | 0 | 11476.1 | 0 | 0 | 0 | 0 | 0 | 0 |
| 60 | 0 | 0 | 0 | 2237.9 | 0 | 1.7 | 3599.6 | 0 | 0 | 0 | 0 | 0 | 0 | 0 |
| 61 | 0 | 0 | 0 | 337 | 0 | 0.2 | 538.6 | 0 | 0 | 0 | 0 | 0 | 0 | 0 |
| 62 | 0 | 0 | 0 | 2673.9 | 0 | 0.2 | 1000 | 0 | 0 | 0 | 0 | 0 | 0 | 0 |
| 70 | 0 | 0 | 0 | 2411.4 | 0 | 21.9 | 0 | 0 | 0 | 4060.4 | 0 | 0 | 0 | 0 |
| 71 | 0 | 0 | 0 | 710.7 | 0 | 18 | 0 | 0 | 0 | 1720.3 | 0 | 0 | 0 | 0 |
| 72 | 0 | 0 | 0 | 0.7 | 0 | 0 | 0 | 0 | 0 | 0.3 | 0 | 0 | 0 | 0 |
| 80 | 0 | 0 | 0 | 2977.6 | 0 | 4 | 0.1 | 0 | 2143.5 | 0 | 0 | 0 | 0 | 0 |
| 81 | 0 | 0 | 0 | 0.7 | 0 | 0 | 0 | 0 | 4.1 | 0 | 0 | 0 | 0 | 0 |
| 82 | 0 | 0 | 0 | 0 | 0 | 0 | 0 | 0 | 0 | 0 | 0 | 0 | 0 | 0 |
| 90 | 0 | 0 | 0 | 441 | 0 | 1.6 | 674.1 | 63.7 | 77.8 | 918.5 | 0 | 0 | 0 | 0 |
| 100 | 0 | 0 | 0 | 2443.7 | 0 | 2.6 | 233.8 | 329.3 | 43.4 | 354 | 0 | 0 | 0 | 0 |
| 110 | 0 | 0 | 0 | 977.3 | 0 | 0.5 | 66.1 | 26.1 | 3.5 | 11.1 | 0 | 0 | 0 | 0 |
| 120 | 0 | 0 | 0 | 7246.3 | 0 | 4 | 176.3 | 125.5 | 3.9 | 80.7 | 1746.8 | 632.9 | 164.7 | 724.5 |
| 121 | 0 | 0 | 0 | 142.5 | 0 | 0 | 1.6 | 26.3 | 5.3 | 0.6 | 2.7 | 31.2 | 26.8 | 1.5 |
| 122 | 0 | 0 | 0 | 1294.6 | 0 | 1.1 | 41 | 68.5 | 10.4 | 4.2 | 211 | 154.6 | 293.8 | 86.8 |
| 130 | 0 | 0 | 0 | 13338.8 | 0 | 5.8 | 144 | 159 | 8.5 | 47.4 | 0 | 0 | 0 | 0 |
| 140 | 0 | 0 | 0 | 1476.9 | 0 | 14.2 | 0 | 0 | 0 | 0 | 0 | 0 | 0 | 0 |
| 150 | 7254.8 | 0 | 0 | 1157.7 | 0 | 20.4 | 0.5 | 1.3 | 0.6 | 12 | 0 | 0 | 0 | 0 |
| 151 | 0 | 0 | 0 | 0 | 0 | 0 | 0 | 0 | 0 | 0 | 0 | 0 | 0 | 0 |
| 152 | 63 | 0 | 0 | 8.9 | 0 | 0.2 | 0.1 | 0 | 0.2 | 1.1 | 0 | 0 | 0 | 0 |
| 153 | 323.8 | 0 | 0 | 52.7 | 0 | 0.1 | 0 | 0 | 0 | 0 | 0 | 0 | 0 | 0 |
| 160 | 0 | 0 | 0 | 200.4 | 0 | 2.3 | 71.7 | 442.6 | 27.4 | 151.4 | 0 | 0 | 0 | 0 |
| 170 | 0 | 0 | 0 | 86.1 | 0 | 5 | 12.3 | 110 | 4.6 | 0.8 | 0 | 0 | 0 | 0 |
| 180 | 0 | 0 | 0 | 1231.9 | 0 | 11.7 | 12.7 | 15.1 | 5.5 | 51.8 | 122.3 | 56.6 | 47.7 | 362.7 |
| 190 | 0 | 476.7 | 0 | 162.5 | 0 | 1.9 | 2.5 | 1.3 | 0.2 | 2.1 | 0 | 0 | 0 | 0 |
| 200 | 19156.9 | 0 | 0 | 0 | 0 | 12.2 | 0.4 | 0 | 0.2 | 0.5 | 0 | 0 | 0 | 0 |
| 201 | 108.8 | 0 | 0 | 0 | 0 | 0.3 | 0 | 0 | 0 | 0 | 0 | 0 | 0 | 0 |
| 202 | 97.2 | 0 | 0 | 0 | 0 | 0.1 | 0 | 0 | 0 | 0 | 0 | 0 | 0 | 0 |
| 210 | 0 | 0 | 0 | 182.6 | 0 | 365991.8 | 7.2 | 8.9 | 3.1 | 31.3 | 0 | 0 | 0 | 0 |
| 220 | 0 | 0 | 0 | 0 | 14694.2 | 0 | 0 | 0 | 0 | 0 | 0 | 0 | 0 | 0 |

**Table 4.** Percentage PFT composition by class for 2010 calculated as an area-weighted mean over all pixels of the class globally.

| Class code | Bare soil | Built | Managed grasses | Natural grasses | Snow/ice | Water[2] | BD trees | BE trees | ND trees | NE trees | BD shrubs | BE shrubs | ND shrubs | NE shrubs |
|---|---|---|---|---|---|---|---|---|---|---|---|---|---|---|
| 10 | 0.0 | 0.0 | 94.9 | 0.0 | 0.0 | 0.0 | 2.1 | 2.5 | 0.0 | 0.4 | 0.0 | 0.0 | 0 | 0.0 |
| 11 | 0.0 | 0.0 | 96.5 | 0.0 | 0.0 | 0.0 | 1.6 | 1.6 | 0.1 | 0.3 | 0.0 | 0.0 | 0 | 0.0 |
| 12 | 0.0 | 0.0 | 81.6 | 0.0 | 0.0 | 0.0 | 2.4 | 15.7 | 0.0 | 0.3 | 0.0 | 0.0 | 0 | 0.0 |
| 20 | 0.0 | 0.0 | 98.8 | 0.0 | 0.0 | 0.1 | 0.8 | 0.3 | 0.0 | 0.1 | 0.0 | 0.0 | 0 | 0.0 |
| 30 | 0.0 | 0.0 | 81.6 | 0.0 | 0.0 | 0.0 | 3.6 | 13.6 | 0.0 | 1.1 | 0.0 | 0.0 | 0 | 0.0 |
| 40 | 0.0 | 0.0 | 43.7 | 35.0 | 0.0 | 0.0 | 5.5 | 13.8 | 0.1 | 1.8 | 0.0 | 0.0 | 0 | 0.0 |
| 50 | 0.0 | 0.0 | 0.0 | 9.9 | 0.0 | 0.0 | 0.0 | 90.1 | 0.0 | 0.0 | 0.0 | 0.0 | 0 | 0.0 |
| 60 | 0.0 | 0.0 | 0.0 | 38.3 | 0.0 | 0.0 | 61.6 | 0.0 | 0.0 | 0.0 | 0.0 | 0.0 | 0 | 0.0 |
| 61 | 0.0 | 0.0 | 0.0 | 38.5 | 0.0 | 0.0 | 61.5 | 0.0 | 0.0 | 0.0 | 0.0 | 0.0 | 0 | 0.0 |
| 62 | 0.0 | 0.0 | 0.0 | 72.8 | 0.0 | 0.0 | 27.2 | 0.0 | 0.0 | 0.0 | 0.0 | 0.0 | 0 | 0.0 |
| 70 | 0.0 | 0.0 | 0.0 | 37.1 | 0.0 | 0.3 | 0.0 | 0.0 | 0.0 | 62.5 | 0.0 | 0.0 | 0 | 0.0 |
| 71 | 0.0 | 0.0 | 0.0 | 29.0 | 0.0 | 0.7 | 0.0 | 0.0 | 0.0 | 70.2 | 0.0 | 0.0 | 0 | 0.0 |

---

[1] For the water body class (code 210), the water PFT area includes 2,877,500 km² of inland water. For all other classes, all water PFT area is inland water.

[2] For the water body class (code 210), the water PFT percentage includes inland water. The area-weighted mean percentage composition of inland water PFT in water body class pixels is 0.8 %. For all other classes, all water is inland water.

| | | | | | | | | | | | | | | |
|---|---|---|---|---|---|---|---|---|---|---|---|---|---|---|
| 72 | 0.0 | 0.0 | 0.0 | 72.6 | 0.0 | 1.3 | 0.0 | 0.0 | 0.0 | 26.1 | 0.0 | 0.0 | 0 | 0.0 |
| 80 | 0.0 | 0.0 | 0.0 | 58.1 | 0.0 | 0.1 | 0.0 | 0.0 | 41.8 | 0.0 | 0.0 | 0.0 | 0 | 0.0 |
| 81 | 0.0 | 0.0 | 0.0 | 15.4 | 0.0 | 0.5 | 0.0 | 0.0 | 84.1 | 0.0 | 0.0 | 0.0 | 0 | 0.0 |
| 82 | 0.0 | 0.0 | 0.0 | 82.9 | 0.0 | 0.0 | 0.0 | 0.0 | 17.1 | 0.0 | 0.0 | 0.0 | 0 | 0.0 |
| 90 | 0.0 | 0.0 | 0.0 | 20.3 | 0.0 | 0.1 | 31.0 | 2.9 | 3.6 | 42.2 | 0.0 | 0.0 | 0 | 0.0 |
| 100 | 0.0 | 0.0 | 0.0 | 71.7 | 0.0 | 0.1 | 6.9 | 9.7 | 1.3 | 10.4 | 0.0 | 0.0 | 0 | 0.0 |
| 110 | 0.0 | 0.0 | 0.0 | 90.1 | 0.0 | 0.0 | 6.1 | 2.4 | 0.3 | 1.0 | 0.0 | 0.0 | 0 | 0.0 |
| 120 | 0.0 | 0.0 | 0.0 | 66.4 | 0.0 | 0.0 | 1.6 | 1.2 | 0.0 | 0.7 | 16.0 | 5.8 | 1.5 | 6.6 |
| 121 | 0.0 | 0.0 | 0.0 | 59.7 | 0.0 | 0.0 | 0.7 | 11.0 | 2.2 | 0.3 | 1.1 | 13.1 | 11.3 | 0.6 |
| 122 | 0.0 | 0.0 | 0.0 | 59.8 | 0.0 | 0.1 | 1.9 | 3.2 | 0.5 | 0.2 | 9.7 | 7.1 | 13.6 | 4.0 |
| 130 | 0.0 | 0.0 | 0.0 | 97.3 | 0.0 | 0.0 | 1.1 | 1.2 | 0.1 | 0.3 | 0.0 | 0.0 | 0 | 0.0 |
| 140 | 0.0 | 0.0 | 0.0 | 99.1 | 0.0 | 0.9 | 0.0 | 0.0 | 0.0 | 0.0 | 0.0 | 0.0 | 0 | 0.0 |
| 150 | 85.9 | 0.0 | 0.0 | 13.7 | 0.0 | 0.2 | 0.0 | 0.0 | 0.0 | 0.1 | 0.0 | 0.0 | 0 | 0.0 |
| 151 | 86.0 | 0.0 | 0.0 | 14.0 | 0.0 | 0.0 | 0.0 | 0.0 | 0.0 | 0.0 | 0.0 | 0.0 | 0 | 0.0 |
| 152 | 85.8 | 0.0 | 0.0 | 12.1 | 0.0 | 0.2 | 0.1 | 0.0 | 0.3 | 1.5 | 0.0 | 0.0 | 0 | 0.0 |
| 153 | 86.0 | 0.0 | 0.0 | 14.0 | 0.0 | 0.0 | 0.0 | 0.0 | 0.0 | 0.0 | 0.0 | 0.0 | 0 | 0.0 |
| 160 | 0.0 | 0.0 | 0.0 | 22.4 | 0.0 | 0.3 | 8.0 | 49.4 | 3.1 | 16.9 | 0.0 | 0.0 | 0 | 0.0 |
| 170 | 0.0 | 0.0 | 0.0 | 39.3 | 0.0 | 2.3 | 5.6 | 50.3 | 2.1 | 0.4 | 0.0 | 0.0 | 0 | 0.0 |
| 180 | 0.0 | 0.0 | 0.0 | 64.2 | 0.0 | 0.6 | 0.7 | 0.8 | 0.3 | 2.7 | 6.4 | 3.0 | 2.5 | 18.9 |
| 190 | 0.0 | 73.7 | 0.0 | 25.1 | 0.0 | 0.3 | 0.4 | 0.2 | 0.0 | 0.3 | 0.0 | 0.0 | 0 | 0.0 |
| 200 | 99.9 | 0.0 | 0.0 | 0.0 | 0.0 | 0.1 | 0.0 | 0.0 | 0.0 | 0.0 | 0.0 | 0.0 | 0 | 0.0 |
| 201 | 99.7 | 0.0 | 0.0 | 0.0 | 0.0 | 0.2 | 0.0 | 0.0 | 0.0 | 0.0 | 0.0 | 0.0 | 0 | 0.0 |
| 202 | 99.9 | 0.0 | 0.0 | 0.0 | 0.0 | 0.1 | 0.0 | 0.0 | 0.0 | 0.0 | 0.0 | 0.0 | 0 | 0.0 |
| 210 | 0.0 | 0.0 | 0.0 | 0.0 | 0.0 | 99.9 | 0.0 | 0.0 | 0.0 | 0.0 | 0.0 | 0.0 | | 0.0 |
| 220 | 0.0 | 0.0 | 0.0 | 0.0 | 100.0 | 0.0 | 0.0 | 0.0 | 0.0 | 0.0 | 0.0 | 0.0 | 0 | 0.0 |

**Data availability**

The CCI PFT dataset 1992-2020 is freely, permanently, and publicly available on a web viewer: http://maps.elie.ucl.ac.be/CCI/viewer/download.php (doi: 10.5285/26a0f46c95ee4c29b5c650b129aab788, Harper et al., 2022).

**Author contribution**

PD conceived the idea and supervised the research effort with contribution from PP. CL coordinated the project. KH designed the methodology with contribution from CL. KH developed the code to generate the CCI PFT dataset 2010. AH, PP, CO, VB, RSM, and SIB designed the modelling experiments and analysed the results. GK, MB, RS, and CB designed and developed the user tool. GK and RS managed and produced the CCI PFT dataset 2010 metadata. KH wrote the original draft with contributions from CL, AH, SIB, PP, and CO. All co-authors reviewed the manuscript.

**Competing interests**

"The authors declare that they have no conflict of interest."

## References

Andrefouet, S., Bindschadler, R., Brown de Colstoun, E., Choate, M., Chomentowski, W., Christopherson, J., ... & Wylie, B. Preliminary Assessment of the Value of Landsat-7 ETM+ Data Following Scan Line Corrector Malfunction. US Geological Survey, EROS Data Center: Sioux Falls, SD, USA, 2003.

Bartsch, A., Widhalm, B., Pointner, G.; Ermokhina, K. A., Leibman, M., Heim, B.: Land cover derived from Sentinel-1 and Sentinel-2 satellite data (2015-2018) for subarctic and arctic environments, Zentralanstalt für Meteorologie und Geodynamik, Wien, PANGAEA, https://doi.org/10.1594/PANGAEA.897916, 2019.

Bastos, A., O'Sullivan, M., Ciais, P., Makowski, D., Sitch, S., Friedlingstein, P., Chevallier, F., Rödenbeck, C., Pongratz, J., Luijkx, I. T., Patra, P. K., Peylin, P., Canadell, J. G., Lauerwald, R., Li, W., Smith, N. E., Peters, W., Goll, D. S., Jain, A. K., Kato, E., Lienert, S., Lombardozzi, D. L., Haverd, V., Nabel, J. E. M. S., Poulter, B., Tian, H., Walker, A. P., and Zaehle, S.: Sources of uncertainty in regional and global terrestrial CO2 exchange estimates, Global Biogeochem. Cycles, 34, 1–21, https://doi.org/10.1029/2019GB006393, 2020.

Bastos, A., Hartung, K., Nützel, T. B., Nabel, J. E. M. S., Houghton, R. A., and Pongratz, J.: Comparison of uncertainties in land-use change fluxes from bookkeeping model parameterisation, Earth Syst. Dyn., 12, 745–762, https://doi.org/10.5194/esd-12-745-2021, 2021.

Beck, H. E., Zimmermann, N. E., McVicar, T. R., Vergopolan, N., Berg, A., and Wood, E. F.: Present and future Köppen-Geiger climate classification maps at 1-km resolution, Nature Scientific Data 5(180214), https://doi.org/10.1038/sdata.2018.214, 2018.

Best, M. J., Pryor, M., Clark, D. B., Rooney, G. G., Essery, R. L. H., Ménard, C. B., Edwards, J. M., Hendry, M. A., Porson, A., Gedney, N., Mercado, L. M., Sitch, S., Blyth, E., Boucher, O., Cox, P. M., Grimmond, C. S. B., and Harding, R. J.: The Joint UK Land Environment Simulator (JULES), model description – Part 1: Energy and water fluxes, Geosci. Model Dev., 4, 677–699, https://doi.org/10.5194/gmd-4-677-2011, 2011.

Bouvet, A., Mermoz, S., Le Toan, T., Villard, L., Mathieu, R., Naidoo, L., and Asner, G. P.: An Above-Ground Biomass Map of African Savannahs and Woodlands at 25 m Resolution Derived from ALOS PALSAR, Remote Sens. Environ., 206, 156–173, https://doi.org/10.1016/j.rse.2017.12.030, 2018.

Box, E. O.: Predicting physiognomic vegetation types with climate variables, Vegetatio 45(2), 127–139, doi:10.1007/BF00119222, 1981.

Box, E. O.: Plant functional types and climate at the global scale, J. Veg. Sci., 7, 309–320, https://doi.org/10.2307/3236274, 1996.

Brovkin, V., Claussen, M., Driesschaert, E., Fichefet, T., Kicklighter, D., Loutre, M. F., Matthews, H. D., Ramankutty, N., Schaeffer, M., and Sokolov, A.: Biogeophysical effects of historical land cover changes simulated by six Earth system models of intermediate complexity, Clim. Dyn., 26, 587–600, https://doi.org/10.1007/s00382-005-0092-6, 2006.

Clark, D.B., Mercado, L.M., Sitch, S., Jones, C.D., Gedney, N., Best, M.J., Pryor, M., Rooney, G.G., Essery, R.L.H., Blyth, E., Boucher, O., Harding, R.J., Huntingford, C., and Cox, P.M. The Joint UK Land Environment Simulator (JULES), model description – Part 2: Carbon fluxes and vegetation dynamics. Geosci. Model Dev., 4, 701–722, doi:10.5194/gmd-4-701-2011, 2011.

Dale, V. H.: The relationship between land-use change and climate change, Ecol. Appl., 7, 753–769, https://doi.org/10.1890/1051-0761(1997)007[0753:TRBLUC]2.0.CO;2, 1997.

Danielson, J., and Gesch, D.: Global Multi-resolution Terrain Elevation Data 2010 (GMTED2010), U.S. Geological Survey Open File Report 2011-1073, doi: 10.3133/ofr20111073, 2011.

Defourny, P., Lamarche, C., Brockmann, C., Boettcher, M., Bontemps, S., De Maet, T., Duveiller, G. L. Harper, K., Hartley A., Kirches, G., Moreau, I., Peylin, P., Ottlé, C., Radoux J., Van Bogaert, E., Ramoino, F., Albergel, C., Arino, O. Observed annual global land-use change from 1992 to 2020 three times more dynamic than reported by inventory-based statistics, submitted, 2022.

Devaraju, N., Bala, G., and Modak, A.: Effects of large-scale deforestation on precipitation in the monsoon regions: Remote versus local effects, Proc. Natl. Acad. Sci. U. S. A., 112, 3257–3262, https://doi.org/10.1073/pnas.1423439112, 2015.

Di Gregorio, A., and Jansen, L. J. M. Land Cover Classification System (LCCS): Classification Concepts and User Manual. Fao (Vol. 53). Food & Agriculture Organization, 2005.

Esch, T., Heldens, W., Hirner, A., Keil, M., Marconcini, M., Roth, A., Zeidler, J., Dech, S., and Strano, E.: Breaking new ground in mapping human settlements from space – The Global Urban Footprint, 134, 30–42, https://doi.org/https://doi.org/10.1016/j.isprsjprs.2017.10.012, 2017.

Feddema, J., Oleson, K., Bonan, G., Mearns, L., Washington, W., Meehl, G., and Nychka, D.: A comparison of a GCM response to historical anthropogenic land cover change and model sensitivity to uncertainty in present-day land cover representations, Clim. Dyn., 25, 581–609, https://doi.org/10.1007/s00382-005-0038-z, 2005.

Foley, J. A., DeFries, R., Asner, G. P., Barford, C., Bonan, G., Carpenter, S. R., Chapin, F. S., Coe, M. T., Daily, G. C., Gibbs, H. K., Helkowski, J. H., Holloway, T., Howard, E. A., Kucharik, C. J., Monfreda, C., Patz, J. A., Prentice, I. C., Ramankutty, N., and Snyder, P. K.: Global consequences of land use, Science (80-. )., 309, 570–574, https://doi.org/10.1126/science.1111772, 2005.

Friedlingstein, P., Jones, M. W., Sullivan, M. O., Andrew, R. M., Bakker, D. C. E., Hauck, J., 688 Quéré, C. Le, Peters, G. P., and Peters, W.: Global Carbon Budget 2021, 1917–2005, 2022.

Frieler, K., Lange, S., Piontek, F., Reyer, C. P. O., Schewe, J., Warszawski, L., et al. Assessing the impacts of 1.5°C global warming - Simulation protocol of the Inter-Sectoral Impact Model Intercomparison Project (ISIMIP2b). Geoscientific Model Development, 10(12), 4321–4345. https://doi.org/10.5194/GMD-10-4321-2017, 2017.

GCOS (Global Climate Observing System), Public Review of GCOS Requirements for Essential Climate Variables Survey. GCOS Review of Requirements for Climate Monitoring. https://gcos.wmo.int/en/essential-climate-variables/table, 2016.

Hansen, M.C., Potapov, P.V., Moore, R., Hancher, M., Turubanova, S.A., Tyukavina, A., Thau, D., Stehman, S.V., Goetz, S.J., Loveland, T.R., Kommareddy, A., Egorov, A., Chini, L., Justice, C.O., and Townshend, J.R.G. High-resolution global maps of 21st-century forest cover change. Science, 342(6160), 850–853, doi: 10.1126/science.1244693, 2013.

Harper K.L., Lamarche, C., Hartley, A., Peylin, P., Ottlé, C., Bastrikov, V., San Martín, R., Bohnenstengel, S.I., Kirches, G., Boettcher, M., Shevchuk, R., Brockmann, C., Defourny, P. A 29-year time series of annual 300-metre resolution plant functional type maps for climate models (v2.0.8). doi: 0.5285/26a0f46c95ee4c29b5c650b129aab788, 2022.

Harris, I., Jones, P.D., Osborn, T.J., and Lister, D.H. Updated high-resolution grids of monthly climatic observations – the CRU TS3.10 Dataset. Int. J. Climatol., 34, 623–642, doi: 10.1002/joc.3711, 2014.

Hartley, A.J., MacBean, N., Georgievski, G., and Bontemps, S. Uncertainty in plant functional type distributions and its impact on land surface models. Remote Sensing of Environment 2013, 71–89, doi: 10.1016/j.rse.2017.07.037, 2017.

Hollmann, R., Merchant, C. J., Saunders, R., Downy, C., Buchwitz, M., Cazenave, A., Chuvieco, E., Defourny, P., De Leeuw, G., Forsberg, R., Holzer-Popp, T., Paul, F., Sandven, S., Sathyendranath, S., Van Roozendael, M., Wagner, W., others, Holzer-Popp, T., Paul, F., Sandven, S., Sathyendranath, S., Van Roozendael, M., and Wagner, W.: The ESA climate change initiative: Satellite data records for essential climate variables, 94, 1541–1552, https://doi.org/10.1175/BAMS-D-11-00254.1, 2013.

Houghton, R.A. Aboveground forest biomass and the global carbon balance, Glob. Chang. Biol. 11, 945–958, doi: 10.1111/j.1365-2486.2005.00955.x, 2005.

Houghton, R.A., House, J.I., Pongratz, J., Van Der Werf, G.R., Defries, R.S., Hansen, M.C., Le Quéré, C., and Ramankutty, N. Carbon emissions from land use and land-cover change, Biogeosciences 9, 5125–5142, doi: 10.5194/bg-9-5125-2012, 2012.

IPCC: Climate Change 2022: Impacts, Adaptation, and Vulnerability. Contribution of Working 744 Group II to the Sixth Assessment Report of the Intergovernmental Panel on Climate Change. [H.-745 O. Pörtner, D.C. Roberts, M. Tignor, E.S. Poloczanska, K. Mintenbeck, A. Ale, 2022.

Jung, M., Henkel, K., Herold, M., and Churkina, G. Exploiting synergies of global land cover products for carbon cycle modeling, Remote Sens. Environ. 101, 534–553, doi: 10.1016/j.rse.2006.01.020, 2006.

Kobayashi, S., Ota, Y., Harada, Y., Ebita, A., Moriya, M., Onoda, H., Onogi, K., Kamahori, H., Kobayashi, C., Endo, H., Miyaoka, K., and Takahashi, K. The JRA-55 Reanalysis: General Specifications and Basic Characteristics, Journal of Meteorological Society of Japan, 93(1), 5–48, doi: 10.2151/jmsj.2015-001, 2015.

Krinner, G., Viovy, N., de Noblet-Ducoudré, N., Ogée, J., Polcher, J., Friedlingstein, P., Ciais, P., Sitch, S., and Prentice, I. C.: A dynamic global vegetation model for studies of the coupled atmosphere-biosphere system, 19, 1–33, https://doi.org/10.1029/2003GB002199, 2005.

Lamarche, C., Santoro, M., Bontemps, S., d'Andrimont, R., Radoux, J., Giustarini, L., Brockmann, C., Wevers, J., Defourny, P., and Arino, O.: Compilation and validation of sar and optical data products for a complete and global map of inland/ocean water tailored to the climate modeling community, 9, https://doi.org/10.3390/rs9010036, 2017.

Lambin, E. F., Turner, B. L., Geist, H. J., Agbola, S. B., Angelsen, A., Bruce, J. W., Coomes, O. T., Dirzo, R., Fischer, G., Folke, C., George, P. S., Homewood, K., Imbernon, J., Leemans, R., Li, X., Moran, E. F., Mortimore, M., Ramakrishnan, P. S., Richards, J. F., Skånes, H., Steffen, W., Stone, G. D., Svedin, U., Veldkamp, T. A., Vogel, C., and Xu, J.: The causes of land-use and land-cover change: Moving beyond the myths, Glob. Environ. Chang., 11, 261–269, https://doi.org/10.1016/S0959-3780(01)00007-3, 2001.

Liu, S., Bond-Lamberty, B., Boysen, L. R., Ford, J. D., Fox, A., Gallo, K., Hatfield, J., Henebry, G. M., Huntington, T. G., Liu, Z., Lovelan, T. R., Norby, R. J., Soh, T., Steiner, A. L., Yuan, W., Zhang, Z., and Zhao, S.: Grand challenges in understanding the interplay of climate and land changes, Earth Interact., 21, 1–43, https://doi.org/10.1175/EI-D-16-0012.1, 2017.

Loarie, S. R., Lobell, D. B., Asner, G. P., and Field, C. B.: Land-Cover and surface water change drive large albedo increases in south america, Earth Interact., 15, 1–16, https://doi.org/10.1175/2010EI342.1, 2011.

Lurton, T., Balkanski, Y., Bastrikov, V., Bekki, S., Bopp, L., Braconnot, P., ... & Boucher, O. Implementation of the CMIP6 Forcing Data in the IPSL-CM6A-LR Model. Journal of Advances in Modeling Earth Systems, 12(4), e2019MS001940, 2020.

Mahmood, R., Pielke, R. A., Hubbard, K. G., Niyogi, D., Dirmeyer, P. A., Mcalpine, C., Carleton, A. M., Hale, R., Gameda, S., Beltrán-Przekurat, A., Baker, B., Mcnider, R., Legates, D. R., Shepherd, M., Du, J., Blanken, P. D., Frauenfeld, O. W., Nair, U. S., and Fall, S.: Land cover changes and their biogeophysical effects on climate, Int. J. Climatol., 34, 929–953, https://doi.org/10.1002/joc.3736, 2014.

Marie, G., Luyssaert, B. S., Dardel, C., Le Toan, T., Bouvet, A., Mermoz, S., ... & Peylin, P. Constraining a land cover map with satellite-based aboveground biomass estimates over Africa. Geoscientific Model Development, 15(6), 2599-2617, 2022.

Mathison et al. (in preparation). Description and Evaluation of the JULES-ES setup for ISIMIP2b.

McGlynn, E., Li, S., Berger, M.F., Amend, M., and Harper, K.L. Addressing uncertainty and bias in land use, land use change, and forestry greenhouse gas inventories. Climatic Change 170, 5, doi: 10.1007/s10584-021-03254-2, 2022.

Pachauri, R. K. and Meyer, L. A.: Climate Change 2014: Synthesis Report. Contribution of Working Groups I, II and III to the Fifth Assessment Report of the Intergovernmental Panel on Climate Change, IPCC, 259–264 pp., 2014.

Pekel, J.-F., Cottam, A., Gorelick, N., and Belward, A.S. High-resolution mapping of global surface water and its long-term changes. Nature, 540, 418–422, doi: 10.1038/nature20584, 2016.

Perugini, L., Caporaso, L., Marconi, S., Cescatti, A., Quesada, B., De Noblet-Ducoudré, N., House, J. I., and Arneth, A.: Biophysical effects on temperature and precipitation due to land cover change, Environ. Res. Lett., 12, https://doi.org/10.1088/1748-9326/aa6b3f, 2017.

998

999 Pesaresi, M., Huadong, G., Blaes, X., Ehrlich, D., Ferri, S., Gueguen, L., Halkia, M., Kauffmann, M., Kemper, T., Lu, L.,
1000 Marin-Herrera, M. A., Ouzounis, G. K., Scavazzon, M., Soille, P., Syrris, V., and Zanchetta, L. A global human settlement
1001 layer from optical HR/VHR RS data: Concept and first results. IEEE Journal of Selected Topics in Applied Earth Observations
1002 and Remote Sensing, 6(5), 2102–2131, doi: 10.1109/JSTARS.2013.2271445, 2013.

1003

1004 Pielke, R. A.: Land use and climate change, Science (80-. )., 310, 1625–1626, https://doi.org/10.1126/science.1120529, 2005.

1005

1006 Pielke, R. A., Pitman, A., Niyogi, D., Mahmood, R., McAlpine, C., Hossain, F., Goldewijk, K. K., Nair, U., Betts, R., Fall, S.,
1007 Reichstein, M., Kabat, P., and de Noblet, N.: Land use/land cover changes and climate: Modeling analysis and observational
1008 evidence, Wiley Interdiscip. Rev. Clim. Chang., 2, 828–850, https://doi.org/10.1002/wcc.144, 2011.

1009

1010 Pitman, A. J., De Noblet-Ducoudré, N., Cruz, F. T., Davin, E. L., Bonan, G. B., Brovkin, V., Claussen, M., Delire, C.,
1011 Ganzeveld, L., Gayler, V., Van Den Hurk, B. J. J. M., Lawrence, P. J., Van Der Molen, M. K., Müller, C., Reick, C. H.,
1012 Seneviratne, S. I., Strengen, B. J., and Voldoire, A.: Uncertainties in climate responses to past land cover change: First results
1013 from the LUCID intercomparison study, Geophys. Res. Lett., 36, 1–6, https://doi.org/10.1029/2009GL039076, 2009.

1014

1015 Plummer, S., Lecomte, P., and Doherty, M.: The ESA Climate Change Initiative (CCI): A European contribution to the
1016 generation of the Global Climate Observing System, Remote Sens. Environ., 203, 2–8,
1017 https://doi.org/10.1016/j.rse.2017.07.014, 2017.

1018

1019 Pongratz, J., Reick, C. H., Houghton, R. A., and House, J. I.: Terminology as a key uncertainty in net land use and land cover
1020 change carbon flux estimates, Earth Syst. Dyn., 5, 177–195, https://doi.org/10.5194/esd-5-177-2014, 2014.

1021

1022 Potapov, P., Li, X., Hernandez-Serna, A., Tyukavina, A., Hansen, M.C., Kommareddy, A., Pickens, A., Turubanova, S., Tang,
1023 H., Edibaldo Silva, C., Armston, J., Dubayah, R., Blair, J.B., and Hofton, M. Mapping global forest canopy height through
1024 integration of GEDI and Landsat data, Remote Sensing of Environment 253, doi: 10.1016/j.rse.2020.112165, 2021.

1025

1026 Poulter, B., Ciais, P., Hodson, E., Lischke, H., Maignan, F., Plummer, S., and Zimmermann, N. E.: Plant functional type
1027 mapping for earth system models, Geosci. Model Dev. Discuss., 4, 2081–2121, https://doi.org/10.5194/gmdd-4-2081-2011,
1028 2011.

1029

1030 Poulter, B., MacBean, N., Hartley, A., Khlystova, I., Arino, O., Betts, R., Bontemps, S., Boettcher, M., Brockmann, C.,
1031 Defourny, P., Hagemann, S., Herold, M., Kirches, G., Lamarche, C., Lederer, D., Ottlé, C., Peters, M., and Peylin, P. Plant
1032 functional type classification for earth system models: Results from the European Space Agency's Land Cover Climate Change
1033 Initiative. Geosci. Model Dev., 8, 2315–2328, doi:10.5194/gmd-8-2315-2015, 2015.

1034

1035 Sampaio, G., Nobre, C., Costa, M. H., Satyamurty, P., Soares-Filho, B. S., and Cardoso, M.: Regional climate change over
1036 eastern Amazonia caused by pasture and soybean cropland expansion, Geophys. Res. Lett., 34, 2007.

1037

1038 Santoro, M.; Cartus, O. (2019): ESA Biomass Climate Change Initiative (Biomass_cci): Global datasets of forest above-ground
1039 biomass for the year 2017, v1. Centre for Environmental Data Analysis, 02 December 2019.
1040 doi:10.5285/bedc59f37c9545c981a839eb552e4084. http://dx.doi.org/10.5285/bedc59f37c9545c981a839eb552e4084

1041

1042 Santoro, M., Cartus, O., Carvalhais, N., Rozendaal, D. M. A., Avitabile, V., Araza, A., de Bruin, S., Herold, M., Quegan, S.,

1043 Rodríguez-Veiga, P., Balzter, H., Carreiras, J., Schepaschenko, D., Korets, M., Shimada, M., Itoh, T., Moreno Martínez, Á.,

1044 Cavlovic, J., Cazzolla Gatti, R., da Conceição Bispo, P., Dewnath, N., Labrière, N., Liang, J., Lindsell, J., Mitchard, E. T. A.,

1045 Morel, A., Pacheco Pascagaza, A. M., Ryan, C. M., Slik, F., Vaglio Laurin, G., Verbeeck, H., Wijaya, A., and Willcock, S.:

1046 The global forest above-ground biomass pool for 2010 estimated from high-resolution satellite observations, Earth Syst. Sci.

1047 Data, 13, 3927–3950, https://doi.org/10.5194/essd-13-3927-2021, 2021.

1048

1049 Sayre, R., Dangermond, J., Frye, C., Vaughan, R., Aniello, P., Breyer, S., Cribbs, D., Hopkins, D., Nauman, R., Derrenbacher,

1050 W., Wright, D., Brown, C., Convis, C., Smith, J., Benson, L., VanSistine, D.P., Warner, H., Cress, J., Danielson, J., Hamann,

1051 S., Cecere, T., Reddy, A., Burton, D., Grosse, A., True, D., Metzger, M., Hartmann, J., N. Moosdorf, N., Dürr, H., Paganini,

1052 M., Defourny, P., Arino, O., Maynard, S., Anderson, M., and Comer, P.: A New Map of Global Ecological Land Units — An

1053 Ecophysiographic Stratification Approach, Association of American Geographers, Washington, DC, 2014.

1054

1055 Sessa, R. Terrestrial Essential Climate Variables: For Climate Change Assessment, Mitigation and Adaptation. (FAO, Ed.)

1056 (H. Dolman). Rome: GTOS-Secr., Food and Agriculture Organization of the United Nations, 2008.

1057

1058 Stehfest, E., van Vuuren, D., Kram, T., Bouwman, L., Alkemade, R., Bakkenes, M., Biemans, H., 846 Bouwman, A., den

1059 Elzen, M., Janse, J., Lucas, P., van Minnen, J., Müller, C., and Prins, A. G.: 847 Integrated Assessment of Global

1060 Environmental Change with IMAGE 3.0. Model description and 848 policy applications, 370 pp., 2014.

1061

1062 Turner, B. L., Moss, R. H., and Skole, D. L.: Relating land use and global land-cover change: a proposal for an IGBP-HDP

1063 core project. A report from the IGBP/HDP Working Group on Land-Use/Land-Cover Change, IGBP Secretariat, 65 pp., 1993.

1064

1065 UNFCCC: Annex to Report of the Conference of the Parties on its twenty-first session, held in Paris from 30 November to 13

1066 December 2015, Addendum. Part two: Action taken by the Conference of the Parties at its twenty-first session,

1067 FCCC/CP/2015/ 10/Add.1 pp., 2016.

1068

1069 University of East Anglia Climatic Research Unit and Harris, I.C. CRU JRA v2.0: A forcings dataset of gridded land surface

1070 blend of Climatic Research Unit (CRU) and Japanese reanalysis (JRA) data; Jan. 1901–Dec. 2018. Centre for Environmental

1071 Data Analysis, 2019. https://catalogue.ceda.ac.uk/uuid/7f785c0e80aa4df2b39d068ce7351bbb

1072

1073 Vitousek, P. M., Ehrlich, P. R., Ehrlich, A. H., and Matson, P. A.: Human Appropriation of the Products of Photosynthesis,

1074 Bioscience, 36, 368–373, 1986.

1075

1076

1077

1078

1079

**Appendix A: complementary information about the CCI PFT dataset description**
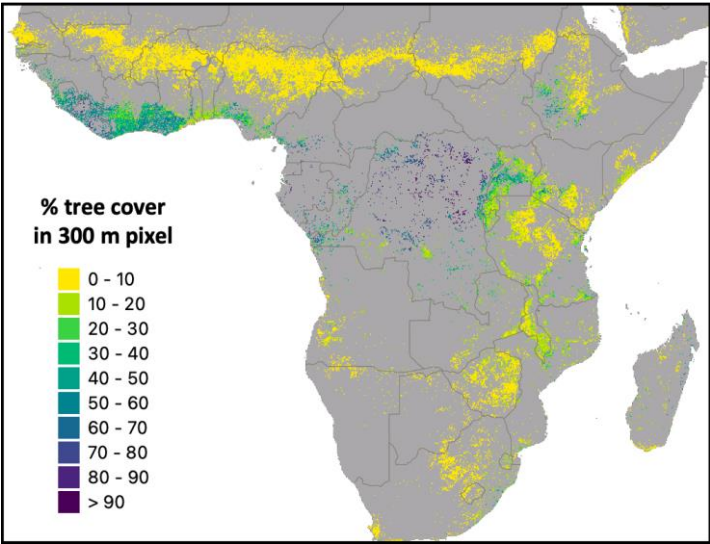
1082 **Figure A1.** Distribution of tree cover percentage in rainfed cropland class pixels in Africa. Gray pixels belong to other classes.

1083
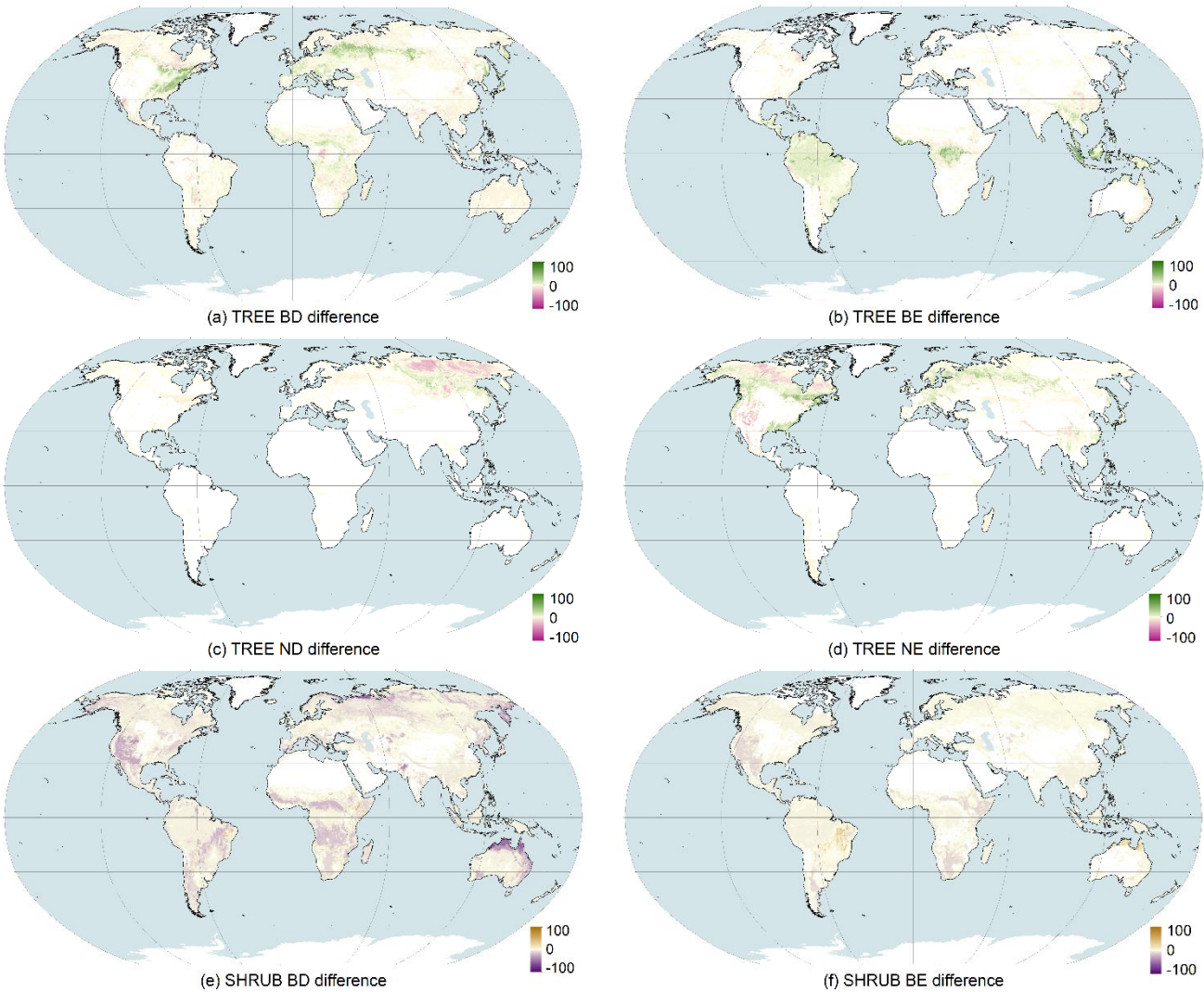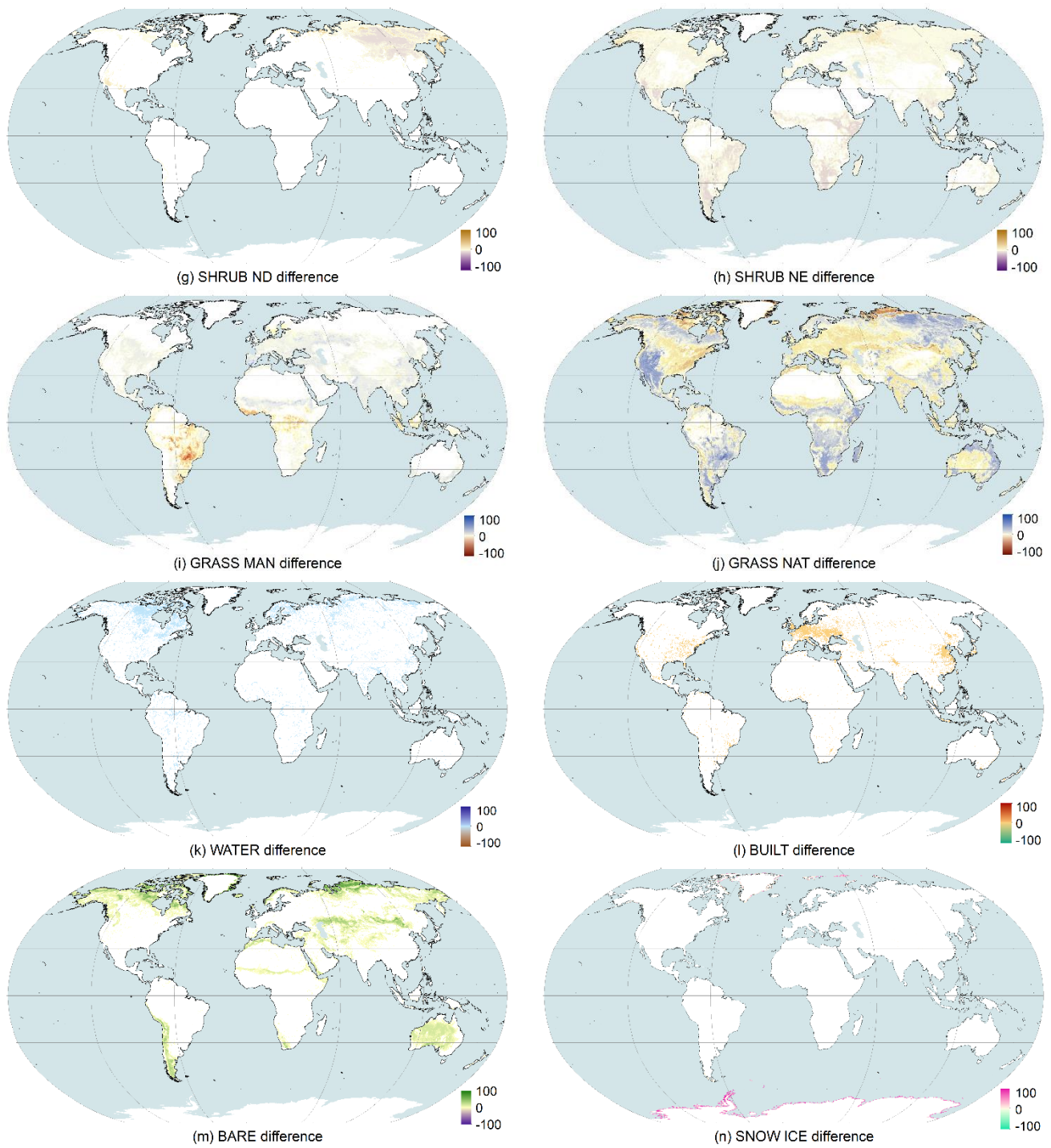


34

**Figure A2.** Absolute differences (percentage of pixel) between the 2010 PFT_local dataset and corresponding PFT_global maps (i.e., applying the global cross-walking scheme) for the 14 PFT types. The spatial resolution is 0.25 x 0.25 degrees.

Figure A3. PFT with the largest increase (a) and largest loss (c) in coverage within 0.25° x 0.25° pixels in the PFT$_{local}$ dataset compared to the PFT$_{global}$ and corresponding fractions gained (b) and lost (d). White areas remained stable in both PFT datasets.

**Table A1.** Global areal cover (1000 km²) of each PFT by land cover class for 2010 based on the most recent version of the global CWT applied to v2.0.8 of the CCI MRLC map.

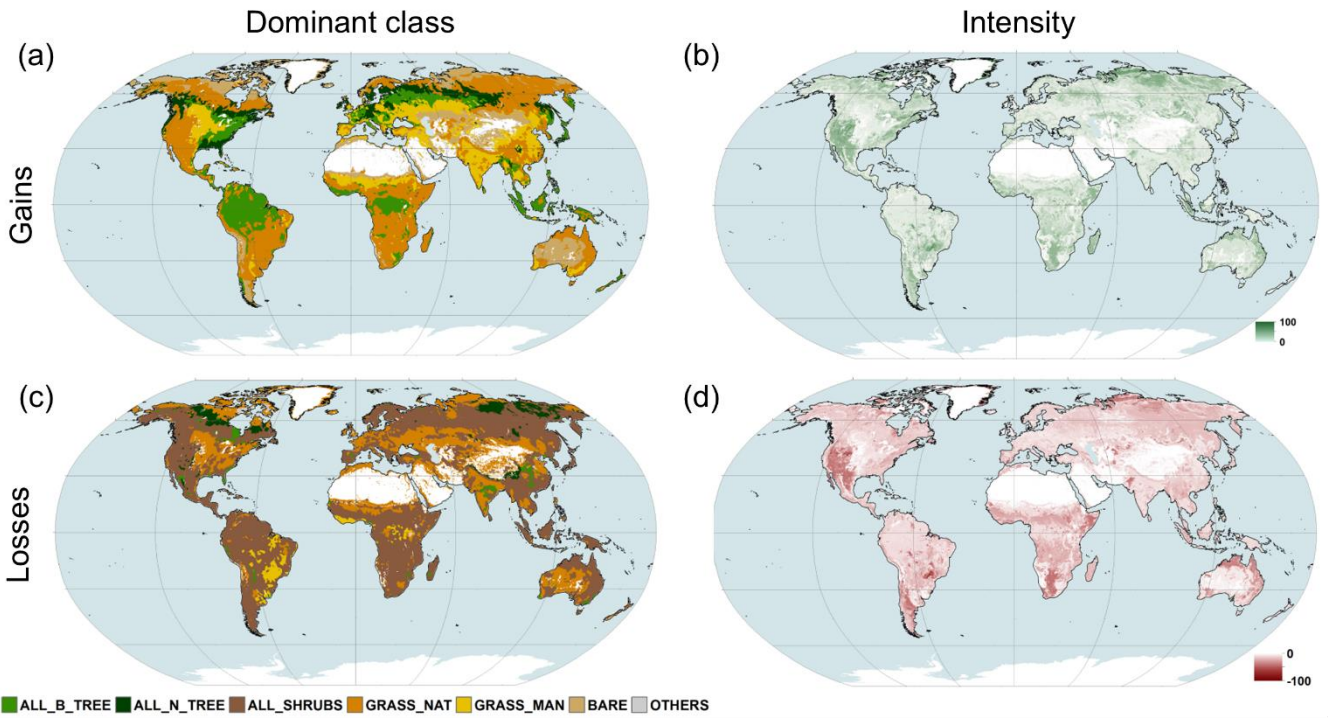| Class | Bare soil | Built | Grass Man | Grass NAT | Snow/ice | Water[3] | BD trees | BE trees | ND trees | NE trees | BD shrubs | BE shrubs | ND shrubs | NE shrubs |
|---|---|---|---|---|---|---|---|---|---|---|---|---|---|---|
| 10 | 0 | 0 | 7328.9 | 814.3 | 0 | 0 | 0 | 0 | 0 | 0 | 0 | 0 | 0 | 0 |
| 11 | 0 | 0 | 6321.2 | 702.4 | 0 | 0 | 0 | 0 | 0 | 0 | 0 | 0 | 0 | 0 |
| 12 | 0 | 0 | 57.1 | 0 | 0 | 0 | 0 | 0 | 0 | 0 | 133.2 | 0 | 0 | 0 |
| 20 | 0 | 0 | 2200.6 | 244.5 | 0 | 0 | 0 | 0 | 0 | 0 | 0 | 0 | 0 | 0 |
| 30 | 0 | 0 | 2060.5 | 515.1 | 0 | 0 | 171.7 | 171.7 | 0 | 0 | 171.7 | 171.7 | 0 | 171.7 |
| 40 | 0 | 0 | 712.9 | 1069.4 | 0 | 0 | 267.4 | 267.4 | 0 | 0 | 534.7 | 356.5 | 0 | 356.5 |
| 50 | 0 | 0 | 0 | 0 | 0 | 0 | 0 | 11468.7 | 0 | 0 | 637.1 | 637.1 | 0 | 0 |
| 60 | 0 | 0 | 0 | 1751.8 | 0 | 0 | 2919.6 | 0 | 0 | 0 | 1167.9 | 0 | 0 | 0 |
| 61 | 0 | 0 | 0 | 131.4 | 0 | 0 | 613.1 | 0 | 0 | 0 | 131.4 | 0 | 0 | 0 |
| 62 | 0 | 0 | 0 | 1653.3 | 0 | 0 | 1102.2 | 0 | 0 | 0 | 918.5 | 0 | 0 | 0 |
| 70 | 0 | 0 | 0 | 974 | 0 | 0 | 0 | 0 | 0 | 4545.6 | 324.7 | 324.7 | 0 | 324.7 |
| 71 | 0 | 0 | 0 | 367.4 | 0 | 0 | 0 | 0 | 0 | 1714.4 | 122.5 | 122.5 | 0 | 122.5 |
| 72 | 0 | 0 | 0 | 0.5 | 0 | 0 | 0 | 0 | 0 | 0.3 | 0 | 0 | 0 | 0.3 |
| 80 | 0 | 0 | 0 | 1537.6 | 0 | 0 | 0 | 0 | 2562.6 | 0 | 128.1 | 128.1 | 640.7 | 128.1 |
| 81 | 0 | 0 | 0 | 0.7 | 0 | 0 | 0 | 0 | 3.4 | 0 | 0.2 | 0.2 | 0 | 0.2 |
| 82 | 0 | 0 | 0 | 0 | 0 | 0 | 0 | 0 | 0 | 0 | 0 | 0 | 0 | 0 |
| 90 | 0 | 0 | 0 | 544.2 | 0 | 0 | 653 | 0 | 217.7 | 435.3 | 108.8 | 108.8 | 0 | 108.8 |
| 100 | 0 | 0 | 0 | 1362.7 | 0 | 0 | 681.4 | 340.7 | 170.3 | 170.3 | 340.7 | 170.3 | 0 | 170.3 |
| 110 | 0 | 0 | 0 | 650.8 | 0 | 0 | 108.5 | 54.2 | 0 | 54.2 | 108.5 | 54.2 | 0 | 54.2 |
| 120 | 2181.1 | 0 | 0 | 2181.1 | 0 | 0 | 0 | 0 | 0 | 0 | 2181.1 | 2181.1 | 0 | 2181.1 |
| 121 | 47.7 | 0 | 0 | 47.7 | 0 | 0 | 0 | 0 | 0 | 0 | 0 | 71.6 | 0 | 71.6 |
| 122 | 433.2 | 0 | 0 | 433.2 | 0 | 0 | 0 | 0 | 0 | 0 | 1299.7 | 0 | 0 | 0 |
| 130 | 0 | 0 | 0 | 13703.6 | 0 | 0 | 0 | 0 | 0 | 0 | 0 | 0 | 0 | 0 |
| 140 | 0 | 0 | 0 | 1491 | 0 | 0 | 0 | 0 | 0 | 0 | 0 | 0 | 0 | 0 |
| 150 | 7180.2 | 0 | 0 | 422.4 | 0 | 0 | 253.4 | 84.5 | 0 | 84.5 | 253.4 | 84.5 | 0 | 84.5 |
| 151 | 0 | 0 | 0 | 0 | 0 | 0 | 0 | 0 | 0 | 0 | 0 | 0 | 0 | 0 |
| 152 | 62.4 | 0 | 0 | 3.7 | 0 | 0 | 0 | 0 | 0 | 0 | 4.4 | 1.5 | 0 | 1.5 |
| 153 | 320.1 | 0 | 0 | 56.5 | 0 | 0 | 0 | 0 | 0 | 0 | 0 | 0 | 0 | 0 |
| 160 | 0 | 0 | 0 | 224 | 0 | 0 | 335.9 | 335.9 | 0 | 0 | 0 | 0 | 0 | 0 |
| 170 | 0 | 0 | 0 | 0 | 0 | 0 | 0 | 164.1 | 0 | 0 | 0 | 54.7 | 0 | 0 |
| 180 | 0 | 0 | 0 | 1150.8 | 0 | 0 | 0 | 0 | 0 | 0 | 479.5 | 0 | 0 | 287.7 |
| 190 | 0 | 647.1 | 0 | 0 | 0 | 0 | 0 | 0 | 0 | 0 | 0 | 0 | 0 | 0 |
| 200 | 19170.2 | 0 | 0 | 0 | 0 | 0 | 0 | 0 | 0 | 0 | 0 | 0 | 0 | 0 |
| 201 | 109.1 | 0 | 0 | 0 | 0 | 0 | 0 | 0 | 0 | 0 | 0 | 0 | 0 | 0 |
| 202 | 97.3 | 0 | 0 | 0 | 0 | 0 | 0 | 0 | 0 | 0 | 0 | 0 | 0 | 0 |
| 210 | 0 | 0 | 0 | 0 | 0 | 366225 | 0 | 0 | 0 | 0 | 0 | 0 | 0 | 0 |
| 220 | 0 | 0 | 0 | 0 | 14694.2 | 0 | 0 | 0 | 0 | 0 | 0 | 0 | 0 | 0 |

[3] For the water body class (code 210), the water PFT area includes 3,110,600 km² of inland water.

1092  **Table A2.** Percentage PFT composition by class based on the most recent update to the global cross-walking table.

| Class code | Bare soil | Built | Managed grasses | Natural grasses | Snow /ice | Water | BD trees | BE trees | ND trees | NE trees | BD shrubs | BE shrubs | ND shrubs | NE shrubs |
|---|---|---|---|---|---|---|---|---|---|---|---|---|---|---|
| 10 | 0 | 0 | 90 | 10 | 0 | 0 | 0 | 0 | 0 | 0 | 0 | 0 | 0 | 0 |
| 11 | 0 | 0 | 90 | 10 | 0 | 0 | 0 | 0 | 0 | 0 | 0 | 0 | 0 | 0 |
| 12 | 0 | 0 | 30 | 0 | 0 | 0 | 0 | 0 | 0 | 0 | 70 | 0 | 0 | 0 |
| 20 | 0 | 0 | 90 | 10 | 0 | 0 | 0 | 0 | 0 | 0 | 0 | 0 | 0 | 0 |
| 30 | 0 | 0 | 60 | 15 | 0 | 0 | 5 | 5 | 0 | 0 | 5 | 5 | 0 | 5 |
| 40 | 0 | 0 | 20 | 30 | 0 | 0 | 7.5 | 7.5 | 0 | 0 | 15 | 10 | 0 | 10 |
| 50 | 0 | 0 | 0 | 0 | 0 | 0 | 0 | 90 | 0 | 0 | 5 | 5 | 0 | 0 |
| 60 | 0 | 0 | 0 | 30 | 0 | 0 | 50 | 0 | 0 | 0 | 20 | 0 | 0 | 0 |
| 61 | 0 | 0 | 0 | 15 | 0 | 0 | 70 | 0 | 0 | 0 | 15 | 0 | 0 | 0 |
| 62 | 0 | 0 | 0 | 45 | 0 | 0 | 30 | 0 | 0 | 0 | 25 | 0 | 0 | 0 |
| 70 | 0 | 0 | 0 | 15 | 0 | 0 | 0 | 0 | 0 | 70 | 5 | 5 | 0 | 5 |
| 71 | 0 | 0 | 0 | 15 | 0 | 0 | 0 | 0 | 0 | 70 | 5 | 5 | 0 | 5 |
| 72 | 0 | 0 | 0 | 45 | 0 | 0 | 0 | 0 | 0 | 30 | 0 | 0 | 0 | 25 |
| 80 | 0 | 0 | 0 | 30 | 0 | 0 | 0 | 0 | 50 | 0 | 2.5 | 2.5 | 12.5 | 2.5 |
| 81 | 0 | 0 | 0 | 15 | 0 | 0 | 0 | 0 | 70 | 0 | 5 | 5 | 0 | 5 |
| 82 | 0 | 0 | 0 | 45 | 0 | 0 | 0 | 0 | 30 | 0 | 0 | 0 | 25 | 0 |
| 90 | 0 | 0 | 0 | 25 | 0 | 0 | 30 | 0 | 10 | 20 | 5 | 5 | 0 | 5 |
| 100 | 0 | 0 | 0 | 40 | 0 | 0 | 20 | 10 | 5 | 5 | 10 | 5 | 0 | 5 |
| 110 | 0 | 0 | 0 | 60 | 0 | 0 | 20 | 10 | 5 | 5 | 10 | 5 | 0 | 5 |
| 120 | 20 | 0 | 0 | 20 | 0 | 0 | 0 | 0 | 0 | 0 | 20 | 20 | 0 | 20 |
| 121 | 20 | 0 | 0 | 20 | 0 | 0 | 0 | 0 | 0 | 0 | 0 | 30 | 0 | 30 |
| 122 | 20 | 0 | 0 | 20 | 0 | 0 | 0 | 0 | 0 | 0 | 60 | 0 | 0 | 0 |
| 130 | 0 | 0 | 0 | 100 | 0 | 0 | 0 | 0 | 0 | 0 | 0 | 0 | 0 | 0 |
| 140 | 0 | 0 | 0 | 100 | 0 | 0 | 0 | 0 | 0 | 0 | 0 | 0 | 0 | 0 |
| 150 | 85 | 0 | 0 | 5 | 0 | 0 | 3 | 1 | 0 | 1 | 3 | 1 | 0 | 1 |
| 151 | 85 | 0 | 0 | 5 | 0 | 0 | 2 | 0 | 2 | 6 | 0 | 0 | 0 | 0 |
| 152 | 85 | 0 | 0 | 5 | 0 | 0 | 0 | 0 | 0 | 0 | 6 | 2 | 0 | 2 |
| 153 | 85 | 0 | 0 | 15 | 0 | 0 | 0 | 0 | 0 | 0 | 0 | 0 | 0 | 0 |
| 160 | 0 | 0 | 0 | 25 | 0 | 0 | 37.5 | 37.5 | 0 | 0 | 0 | 0 | 0 | 0 |
| 170 | 0 | 0 | 0 | 0 | 0 | 0 | 0 | 75 | 0 | 0 | 0 | 25 | 0 | 0 |
| 180 | 0 | 0 | 0 | 60 | 0 | 0 | 0 | 0 | 0 | 0 | 25 | 0 | 0 | 15 |
| 190 | 0 | 100 | 0 | 0 | 0 | 0 | 0 | 0 | 0 | 0 | 0 | 0 | 0 | 0 |
| 200 | 100 | 0 | 0 | 0 | 0 | 0 | 0 | 0 | 0 | 0 | 0 | 0 | 0 | 0 |
| 201 | 100 | 0 | 0 | 0 | 0 | 0 | 0 | 0 | 0 | 0 | 0 | 0 | 0 | 0 |
| 202 | 100 | 0 | 0 | 0 | 0 | 0 | 0 | 0 | 0 | 0 | 0 | 0 | 0 | 0 |
| 210 | 0 | 0 | 0 | 0 | 0 | 100 | 0 | 0 | 0 | 0 | 0 | 0 | 0 | 0 |
| 220 | 0 | 0 | 0 | 0 | 100 | 0 | 0 | 0 | 0 | 0 | 0 | 0 | 0 | 0 |

1093

1094 **Appendix B: complementary information about the modelling results**
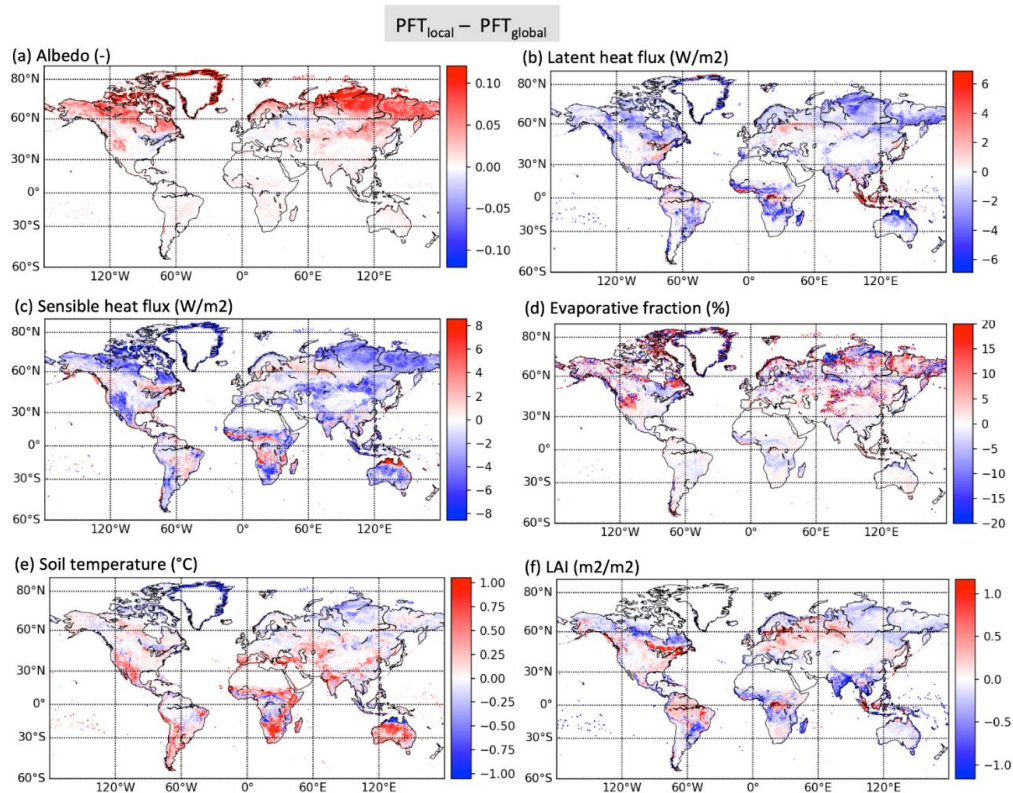


1095

1096 **Figure B1.** Differences in albedo (a), latent heat flux (b), sensible heat flux (c), evaporative fraction (d: Latent heat flux / (Latent + Sensible
1097 heat fluxes), soil surface temperature (e) and Leaf Area Index (LAI, f) simulated by the ORCHIDEE model between the new PFT and the
1098 old PFT distributions, for the annual mean of year 2010 (same as figure 4 but for the annual mean).

1099 **Appendix C: the original default land cover to plant functional type cross-walking table**

1100 **Table C1.** Default land cover to plant functional type cross-walking table provided by the conversion tool with the level 1 UNLCCS
1101 classes and level 2 UNLCCS sub-classes in italics. The units are % coverage of each PFT per UNLCCS class (from Poulter et al., 2015).

| Code | UN LCCS Land Cover Class Description | Trees | | | | Shrubs | | | | Grasses | | Non-vegetated | | |
|------|-------------------------------------|-------|------|------|------|--------|------|------|------|--------|-------|-----------|-------|----------|
| | | Br Ev | Br De | Ne Ev | Ne De | Br Ev | Br De | Ne Ev | Ne De | Nat Gr | Crops | Bare Soil | Water | Snow/ Ice |
| 10 | Cropland, rainfed | | | | | | | | | | 100 | | | |
| *11* | *Herbaceous cover* | | | | | | | | | | *100* | | | |
| *12* | *Tree or shrub cover* | | | | | | *50* | | | | *50* | | | |
| 20 | Cropland, irrigated or post-flooding | | | | | | | | | | 100 | | | |
| 30 | Mosaic cropland (>50 %) / natural vegetation (tree, shrub, herbaceous cover) (<50 %) | 5 | 5 | | | 5 | 5 | 5 | | 15 | 60 | | | |
| 40 | Mosaic natural vegetation (tree, shrub, herbaceous cover) (>50 %) / cropland (<50 %) | 5 | 5 | | | 7.5 | 10 | 7.5 | | 25 | 40 | | | |
| 50 | Tree cover, broadleaved, evergreen, closed to open (>15 %) | 90 | | | | 5 | 5 | | | | | | | |
| 60 | Tree cover, broadleaved, deciduous, closed to open (>15 %) | | 70 | | | | 15 | | | 15 | | | | |
| *61* | *Tree cover, broadleaved, deciduous, closed (>40 %)* | | *70* | | | | *15* | | | *15* | | | | |

38

| Code | UN LCCS Land Cover Class Description | Trees | | | | Shrubs | | | | Grasses | | Non-vegetated | | |
|---|---|---|---|---|---|---|---|---|---|---|---|---|---|---|
| | | Br Ev | Br De | Ne Ev | Ne De | Br Ev | Br De | Ne Ev | Ne De | Nat Gr | Crops | Bare Soil | Water | Snow/Ice |
| *62* | *Tree cover, broadleaved, deciduous, open (15-40 %)* | | *30* | | | | *25* | | | *35* | | *10* | | |
| 70 | Tree cover, needleleaved, evergreen, closed to open (>15 %) | | | 70 | | 5 | 5 | 5 | | 15 | | | | |
| *71* | *Tree cover, needleleaved, evergreen, closed (>40 %)* | | | *70* | | *5* | *5* | *5* | | *15* | | | | |
| *72* | *Tree cover, needleleaved, evergreen, open (15-40 %)* | | | *30* | | | *5* | *5* | | *30* | | *30* | | |
| 80 | Tree cover, needleleaved, deciduous, closed to open (>15 %) | | | | 70 | 5 | 5 | 5 | 0 | 15 | | | | |
| *81* | *Tree cover, needleleaved, deciduous, closed (>40 %)* | | | | *70* | *5* | *5* | *5* | | *15* | | | | |
| *82* | *Tree cover, needleleaved, deciduous, open (15-40 %)* | | | | *30* | | *5* | *5* | *0* | *30* | | *30* | | |
| 90 | Tree cover, mixed leaf type (broadleaved and needleleaved) | | 30 | 20 | 10 | 5 | 5 | 5 | | 15 | | 10 | | |
| 100 | Mosaic tree and shrub (>50 %) / herbaceous cover (<50 %) | 10 | 20 | 5 | 5 | 5 | 10 | 5 | | 40 | | | | |
| 110 | Mosaic herbaceous cover (>50 %) / tree and shrub (<50 %) | 5 | 10 | 5 | | 5 | 10 | 5 | | 60 | | | | |
| 120 | Shrubland | | | | | 20 | 20 | 20 | | 20 | | 20 | | |
| *121* | *Shrubland evergreen* | | | | | *30* | | *30* | | *20* | | *20* | | |
| *122* | *Shrubland deciduous* | | | | | | *60* | | | *20* | | *20* | | |
| 130 | Grassland | | | | | | | | | 60 | | 40 | | |
| 140 | Lichens and mosses | | | | | | | | | 60 | | 40 | | |
| 150 | Sparse vegetation (tree, shrub, herbaceous cover) (<15 %) | 1 | 3 | 1 | | 1 | 3 | 1 | | 5 | | 85 | | |
| *151* | *Sparse tree (<15 %)* | | *2* | *6* | *2* | | | | | *5* | | *85* | | |
| *152* | *Sparse shrub (<15 %)* | | | | | *2* | *6* | *2* | | *5* | | *85* | | |
| *153* | *Sparse herbaceous cover (<15 %)* | | | | | | | | | *15* | | *85* | | |
| 160 | Tree cover, flooded, fresh or brakish water | 30 | 30 | | | | | | | 20 | | | 20 | |
| 170 | Tree cover, flooded, saline water | 60 | | | | 20 | | | | | | | 20 | |
| 180 | Shrub or herbaceous cover, flooded, fresh/saline/brakish water | | 5 | 10 | | | 10 | 5 | | 40 | | | 30 | |
| 190 | Urban areas | | 2.5 | 2.5 | | | | | | 15 | | 75 | 5 | |
| 200 | Bare areas | | | | | | | | | | | 100 | | |
| *201* | *Consolidated bare areas* | | | | | | | | | | | *100* | | |
| *202* | *Unconsolidated bare areas* | | | | | | | | | | | *100* | | |
| 210 | Water bodies | | | | | | | | | | | | 100 | |
| 220 | Permanent snow and ice | | | | | | | | | | | | | 100 |

1102